

Hydrogen Control Calculations for the Sequoyah Plant Station Blackout Scenario

1 Introduction

The Sequoyah containment is equipped with system of igniters designed to ensure a controlled burning of hydrogen in the unlikely event that excessive quantities of hydrogen are generated and released to the containment during a postulated degraded core accident. The igniters operate as hermetically sealed thermal igniters. Power is supplied directly to the igniter at 120-V ac.

During station blackout accident scenarios, offsite and onsite power to the igniters will be interrupted; therefore the igniters will not be available as a hydrogen control system. The series of calculations discussed in this report addresses hydrogen distribution and burn behavior in the Sequoyah containment should onsite power be provided to igniters and/or air return fans during a station blackout accident. For the calculations, the water, steam, and hydrogen sources to the containment have been obtained from a MELCOR calculation of a short-term station blackout accident with pump seal leakage (250 gpm leakage). The MELCOR calculation for this accident is described in the Sandia report "Hydrogen Source Terms for Station Blackout Accidents in Sequoyah and Grand Gulf Estimated Using MELCOR 1.8.5," dated July 26, 2001.

The calculations in this report have been performed by de-coupling the MELCOR reactor cooling system (RCS) models from the containment model, analyzing the containment response as a standalone problem. This de-coupling procedure is required in order to unburden the containment analysis by the time consuming calculations performed in the CORE package of a combined RCS and containment response calculation. Because feedback from the containment system to the RCS is very weak, this type of de-coupling can be accomplished without affecting the source terms (water, steam, and hydrogen) to the containment and the subsequent containment response.¹ Within the MELCOR flow path package, there are features that have been specifically added to the code input that allow the type of de-coupling discussed here.

In the follow discussion, a number of hydrogen control scenarios are explored:

- Delayed deflagration without power to either igniters or fans
- Controlled burning with power to igniters
- Controlled burning with power to igniters and fans.

Various cases are calculated using a variety of MELCOR containment nodalizations and assumptions regarding the ice bed bypass leakage flows. Other uncertainties, including source terms and hydrogen burning parameters, are being planned as additional

¹ A fully coupled calculation is required to account for the affect that small releases of radioactive nuclides have on the containment response. The analysis of these types of second order effects will be addressed in a subsequent report.

calculations to be performed during the next month. In addition, the completed work will include accident time periods extending out to 24 hours. This extended period will therefore include ex-vessel core-concrete interaction (CCI) phenomena that produces a significant amount of late time hydrogen in the containment. For this report, we concentrate only on conditions up to and including vessel failure. This report is therefore preliminary, but does provide insight into some important issues regarding the benefits of providing power to igniters and/or fans during station blackout accidents.

In section 2, the MELCOR reference containment models are described, along with the source terms obtained from a MELCOR RCS/containment station blackout calculation. Hydrogen distribution in the containment and containment pressurization as a result of delayed deflagrations occurring without power to igniters or fans is discussed in Section 3. Section 4 covers the hydrogen controlled burning scenarios when power is supplied to igniters only. Section 5 includes a discussion of those calculations that show the benefit of applying power to both igniters and fans. Section 6 provides a brief summary of these preliminary studies and reflects on work yet to be done.

2 MELCOR Sequoyah Containment Model (s)

Shown in Figure 1 is a drawing of the Sequoyah containment indicating boundaries of three major containment compartments: lower containment, ice-condenser, and upper containment. The ice bed is isolated from the lower and upper containment by lower plenum, intermediate, and upper plenum doors that remain shut during normal operation. During postulated accident events leading to RCS injections of water and steam to the lower containment, these doors can open as a result of the pressure differentials across the doors. Steam flowing into the ice condenser is condensed onto ice baskets holding flakes of ice. The ice bed is therefore a region of low steam concentration, and a probable location for high concentrations of released hydrogen in the case of degraded core accidents. There are no igniters located in the ice bed, and therefore any burns in this regions must be initiated as a result of flame propagation.

An important concern for low steam rate injections is the amount of bypass air and steam flows that go directly from the lower to upper containment compartments. The bypass areas are divided into 1) deck leakage pathways, and 2) refueling drain openings. In the case of the latter, the location and size of the pathways is known. For deck leakage, only an estimate of the maximum amount of leakage is documented in the plant FSAR. Additionally, the location of the deck leakage paths is unknown. In the containment models, these bypass flows are included. Uncertainty in the leakage modeling is addressed with sensitivity calculations.

2.1 Nodalization

Figure 2 is a sketch of a containment model indicating the various sub-compartments that are modeled in one of the MELCOR reference containment models, referred to here as the 26-cell model. In the July 2001 report mentioned above, a reduced nodal model was used for the containment; this model had 12 compartments. Table 1 presents a comparison of these MELCOR reference containment models. Both models were derived from previously documented CONTAIN models of the Sequoyah containment as reported in NUREGs 5586 and 6247. There are major differences between the reference nodalizations that require comment. The 26-cell input deck provides added resolution of the lower containment, ice bed, and upper containment over the 12-cell model. The resolution of the lower containment allows for an improved partitioning of sources according to the local regions where the RCS injections are located. Additionally, the circumferential segmentation of the ice bed allows for asymmetrical melting of ice located in the horseshoe shaped condenser that wraps around most of the lower containment, as shown in Figure 2. The vertical segmentation in the upper containment with the 26-cell model allows for the possibility of upper containment stratification of air and hydrogen in the dome. Since each model is referred to in the discussion below it is worthwhile to mention that there have been some recent revisions to the original MELCOR models in preparation for this work. These revisions are described in Table 2.

Clearly, nodalization of the containment represents a potential source of uncertainty for calculating hydrogen distributions and deflagrations. The concern over nodalization is of course more serious for cases where the air return fans are inoperative. To more fully address the nodalization issue we have added two additional containment models having 15 and 38 compartments. The models are modifications of the 12 and 26-cell models, where the respective ice bed representations are divided into four vertical levels. In the case of the 12-cell model, this segmentation adds an additional three cells in the ice bed model; for the 26-cell model, each circumferential partition in the ice bed is divided into four vertical sections, adding 12 cells to the ice bed representation. Shown in Figures 3 and 4 are the sketches of the ice bed nodalizations investigated in this work. The adaptations of the MELCOR reference models (Figure 4) do behave quite differently in terms of estimated hydrogen distributions and deflagrations. The differences are discussed Sections 3 and 4. A few comments concerning ice bed nodalization and validation (ice melting rates, etc.) are worthwhile here:

- The use of vertical segmentation of the ice bed (Figure 4a) has been validated for ice melting in the CONTAIN code qualification program using Waltz Mill test data. However, this segmentation usage was only valid during rapid blowdown periods where there are large pressure-driven forces, with the associated dominant 1-D vertical flows. Long-term ice bed responses with smaller steam injection flows have been validated only with fans operative, using a single cell to representation of the ice bed. The ice melt data for these long-term scenario cases are only approximate due to the limited degree of instrumentation.

- Waltz Mill test data is applicable mainly to conditions that favor 1-D vertical flows in the ice bed, due to the design of the facility.
- Cross-flow area and loss coefficients for ice beds are derived from geometrical representations of the ice bed and loss coefficient formulas. Unlike the vertical air flow testing conducted in the Waltz Mill facility to obtain experimental loss coefficients, a similar test database for cross-flow does not appear to exist. The lack of experimental data on ice bed cross-flow is a source of some uncertainty in both the 26-cell and 38-cell models: this is recognized. The impact of this uncertainty is believed to be minor due the large density differences that can develop. Sensitivity calculations reflecting on this opinion are not reported here: they will be included in the final report.

2.2 Source terms

The injection rates and integral amounts of water, steam, and hydrogen sourced into the lower compartment for a short-term station blackout accident with pump seal leakage are shown in Figure 5, 6, and 7, respectively. These sources are equivalent to the sources described in the Sandia report for the case referred to as “STSBO-L1.”

From Figure 7, it can be seen that there are two phases to the hydrogen source: the first phase, responsible for approximately half of the total ~ 500 kg of hydrogen released, is primarily injected from the pump seal leakages over about a 30 minutes period prior to hot leg failure. The water and steam injections during this period are relatively small. When the hot leg of the RCS fails due to creep rupture, an additional ~250 kg of hydrogen is released along with a surge of water and steam which rapidly pressurizes the containment. Following the hot leg rupture, the sources to the containment are again relatively small and the containment depressurizes somewhat as it cools before lower head failure at approximately 5.4 hours into the accident.

3 Delayed Deflagration without Power

Without controlled hydrogen burning there is a risk that hydrogen will accumulate in the containment and possibly ignite at a time when a “global” deflagration will be severe enough to threaten the integrity of the containment. For the Sequoyah containment, the pressure corresponding to an estimated 10% failure probability is 525 kPa (absolute).² In addition to the risk of over-pressurizing the containment from a delayed global deflagration, for instance, at the time of vessel failure, there are also other concerns. Local pockets of high hydrogen concentrations in the containment could if ignited produce an accelerated flame, deflagration to detonations transition (DDT), or in some cases a detonation directly. The criteria for DDT and/or detonations are complex; however, it is generally believed that where the hydrogen concentration is 14% (volume fraction) or higher there is a substantial risk of detonation. In some cases, detonations have been observed with hydrogen concentrations as low as 10-12%. In the following

² See Table B.4 in NUREG 6247 for ice condenser containment fragility measures.

analysis we assess 1) the hydrogen distribution within the containment for a local combustion event (DDT or detonation) and 2) over-pressurization of the containment from a global deflagration occurring at the time of vessel failure. Uncertainties in the calculations are noted for the representation of the containment (nodalization) and the assumption made for the bypass flow area.

3.1 Nodalization

Shown in Figure 8 and 9 are containment pressure and temperature profiles for a delayed deflagration scenario. These profiles were calculated using the 26-cell containment model. Essentially, identical profiles are obtained using the 12-cell containment model. However, in the case of the 15-cell model where the ice bed is vertically divided, with no circulation between cells allowed, a very different pressure profile is obtained as shown in Figure 10. Without circulation in the ice bed, large pockets of air accumulate in the upper regions of the ice bed which increases the upper level gas density significantly. For example, the air density in the ice bed for the 15-cell model is approximately 2-3 times that calculated with the 26-cell model (with complete vertical mixing). These density profiles are shown in Figures 11 and 12. The unstable mixture condition develops for the 15-cell model during the early phase of the accident when there are small but protracted steam injections into the lower containment from the pump seal leakage. When the air density is high in the ice bed, the hydrostatic head that must be overcome to force open the lower plenum doors increases. When the head is too high, lower containment gases are vented mainly through the bypass pathways rather than through the ice condenser. Increased steam bypass flow produces the observed rise in the containment pressure. Additionally, since there is no return air flow through the bypass pathways from the upper containment, as in the case for the 26-cell model, the oxygen concentration in the lower containment decreases significantly as the steam concentration correspondingly increases. This situation creates a lower containment condition that cannot support deflagrations. Shown in Figures 13 and 14 are the bypass flows for the 15-cell and 26-cell containment models. The deflagration responsible for the relatively small overpressure at vessel breach (VB) is reduced compared to other modeling cases that allow (or assume) recirculation in the ice bed. The reduce overpressurization due to deflagration at VB in the 15-cell case is the result of 1) a reduced amount of hydrogen present in the upper containment at VB, and 2) the inability to burn hydrogen in the lower containment.

In general, the 12, 26, and 38-cell containment models give very similar results for hydrogen distribution through the containment. Shown in Figures 15 through 17 and in Figures 18 through 20 are the lower and upper containment gas concentrations for each containment model, respectively. Hydrogen gas concentrations in the ice bed for each containment model are shown in Figures 21 through 23.

Because the 26 and 38-cell containment models produce essentially similar concentration profiles, with the 12-cell being a representative average of the more detail nodalizations, we focus our discussion to the 26 and 38-cell model results for most of the remaining report.

The hydrogen concentration profiles in the containment prior to the assumed delayed deflagration are observed to be in the range where the risk of a severe deflagration leading to a detonation is possible if not likely should hydrogen control be unavailable. This is especially the case for the ice bed where maximum hydrogen concentrations of 20-30% are predicted.

3.2 Bypass Pathways

Two sensitivity calculations are presented here for bypass pathway uncertainty. Figures 24 through 26 show the lower containment (cell 9), upper containment (cell 24) and ice bed (cell 18) hydrogen concentrations for the bypass flow area 1) modeled as in the reference 26-cell containment case (0.29 m² at 20 meter elevation), 2) reduced by factor of ten, and 3) with the area elevation changed from 20 to 13 meters elevation. In general, variation in the bypass pathway as described does not have a major impact on the hydrogen distribution either throughout the containment, or specifically in the lower containment. In all three cases considered here we note that there is return air flow from the upper containment to the lower containment maintained through the refueling drains. This return flow is indicated in Figures 27 through 29. Notice in these figures that the air flow through the refueling drains terminates at about 4.3 hours when the lower containment water level reaches the bottom of the drains.

3.3 Ice Melt-out

In addition to hydrogen distributions, we also are interested in the ice melt-out amounts since the presence of ice or lack of ice can affect the level of steam concentration (and inerting) in the condenser at later times. Shown in Figure 30 is the ice melting amounts for each of the four ice bed compartments in the 26-cell containment model. The asymmetric melting profile resulting from the variations in the steam injections are clearly indicated. For comparison, the ice melting amount for the 12-cell containment model is also shown in Figure 31 (single ice bed compartment). We note that only for one circumferential compartment, cell # 19, is the ice completely melted out at the time of vessel breach.

4 Controlled Burning with Power to Igniters

For controlled burning with power to the igniters only, we focus on the 26 and 38-cell containment models. The issues addressed are 1) whether controlled burning can remove a significant amount of hydrogen from the containment without itself creating a severe pressure loading of the containment (i.e. pressure > ~ 500 kPa), and 2) can the controlled burning reduce the risk of DDT or detonations in compartments where, as indicated in Section 2, hydrogen may accumulate (for example, in the ice bed). For the ignition of hydrogen, we use the combustion and propagation limits listed in Table 3. Locations for the igniters are shown in Table 4.

4.1 26-cell Containment Model.

The pressure and temperature profiles in the upper containment with power to igniters only are shown in Figures 32 and 33, respectively. The total amount of hydrogen consumed during the controlled burning is 320 kg, or approximately 2/3 of the hydrogen sourced into the containment up to and including vessel failure. Hydrogen consumed in the lower containment, ice condenser, and upper containment is plotted in Figures 34 through 36, for each of the compartments in the various regions. For the lower containment, approximately 100 kg of hydrogen are consumed by controlled burning. Within the low containment region, the most hydrogen burned is in compartment #8, ~ 42 kg. In ice condenser, ~ 212 kg of hydrogen are consumed. Of this amount, 161 kg are burned in the ice bed itself. Only a few kilograms of hydrogen are consumed in the upper containment, ~8 kg. The burning pattern begins with ignition in the upper plenum region which then propagates downward into the ice bed. Burning in the lower containment begins in compartment #8, about 1.5 minutes after the first burn in the upper plenum. The lower containment burn begins as a result of igniter initiation, not as a result of flame propagation. The steam generator doghouses #2 and #3, burn due to upward flame propagation. Steam generator doghouses #4 and #5 do not have deflagrations. Essentially, all burns in the lower containment terminate with the hot leg failure. The large release of steam accompanying hot leg failure inerts the lower containment, reduces the hydrogen concentration below 5%, and effectively evacuates out most of the oxygen that could sustain a deflagration. Therefore, for times after the hot leg failure, and up to and including vessel failure, the igniters in the lower containment are ineffective, from the standpoint that atmospheric conditions in the region can not support deflagrations.

Shown in Figures 37 through 39 are the hydrogen (6), oxygen (4), and steam (3) concentrations for representative compartments in the upper plenum, ice bed, and lower containment regions. Hydrogen concentrations in the upper containment compartments and ice bed are shown in Figures 40 and 41, respectively. A comparison of the peak hydrogen concentrations for the ice bed and upper containment, with and without power to igniters, show that igniters are effective in controlling hydrogen concentrations in those regions where oxygen content and low steam concentration favor deflagrations. For example, in the upper containment, without the igniters, maximum hydrogen concentrations were in the 10-12% range; with igniters, the maximum concentrations drop to ~ 4%. For the ice bed, the maximum hydrogen concentration without igniters ranged from 20-30%; with igniters, maximum concentrations were limited to less than ~ 10% (except for brief periods associated with rapid steam injections). In the lower containment, maximum hydrogen concentrations ranged from 10-17% without igniters, but were reduced to approximately 5% with igniters.

One concern regarding these calculations is the potential inerting of the lower containment during the initial hydrogen injection from the pump seals, which could 1) reduce the amount of hydrogen consumed in controlled burning, and 2) lead to local high concentrations of hydrogen in the ice bed (a combination of less hydrogen consumed and the absence of upward flame propagation into the ice bed). We saw, for instance, in Figure 39 that the lower containment is steam inerted during an early period when steam

and some hydrogen is being released from the pump seals. De-inerting and burning occurs in the lower containment, just prior to the burst of hydrogen into the containment when the hot leg ruptures. Lower containment burning may be dependent on the proportions of steam and hydrogen released from the seals. With the 26-cell model, we noted that the lower containment can only support deflagration ignition prior to the time when the hot leg fails and large amounts of steam is released. The situation regarding lower containment deflagration is therefore sensitive to both the amount and composition of the pump seal source and the details of the containment modeling. The sensitivity to the source term will be addressed in a subsequent report. Controlled burn sensitivity to containment modeling, specifically for the model that includes vertical segmentation of the ice bed, as described for the 38-cell containment model is discussed below.

4.2 38-cell Containment Model

The 38-cell containment model was developed to provide additional resolution for atmospheric conditions in the ice bed. As noted in Section 3, both the 26 and 38-cell models predict similar results for the upper containment pressure and temperature without power to igniters. With power to igniters only, we observe again nearly identical pressure and temperature profiles for the upper containment. For example, the pressure profile for the 38-cell model with igniters, shown in Figure 42, compares favorably with the profile shown in Figure 32.

As in the case with the 26-cell model, the hydrogen concentration in the upper containment is effectively controlled through the use of igniters. Shown in Figure 43 is gas and steam concentrations in the upper containment, obtained using the 38-cell containment model.

Although the comparison of results from the two containment models are similar, there are variations in the burn patterns between the 26 and 38-cell models, as shown in Table 5. The most notable change is that there is less hydrogen consumed in the lower containment with the 38-cell model. This behavior reflects the sensitivity of lower containment steam and inerting effect to containment modeling. Vertical segmentation of the ice bed increases slightly the flow resistance and gravity head that must be overcome for steam and hydrogen flows into the ice condenser. Small changes in these can also affect the amount of return air flow (from bypass and drains) from the upper containment. The combined effects (flow into the ice condenser and upper containment return flow) can alter the atmospheric conditions enough so that deflagrations in the lower containment are either supported or limited. The variation that is observed does not however affect substantially the behavior of the controlled burns. For example, we see in Figure 43 that hydrogen concentration is only slightly higher for the 38-cell than the 26-cell model when ignition occurs in compartment #10, ~ 19%. We note that for the 26-cell model, ignition occurs at about 17%.

For the ice bed, even with the increased “resolution” afforded by the additional compartments, we see that the hydrogen concentration profiles are very similar to those predicted with the 26-cell model. Shown in Figures 44 and 45, for example, are the

hydrogen concentrations in the lower and upper levels of the ice bed. These concentration values compare favorably with those shown in Figure 41, obtained using the 26-cell model. For the remaining studies on hydrogen distribution and deflagration the 26-cell model will be used.

5 Controlled Burning with Power to Igniters and Fans

In Section 4, calculations were presented indicating that for the station blackout scenario with pump seal leakage, power supplied to the igniters can cause the controlled burning of $\sim 2/3$ of the reactor system's released hydrogen, prior to and including vessel breach. However, there were some regions in the containment, lower containment and ice bed particularly, where hydrogen concentrations rose to $\sim 14\%$. These instances were mainly the result of local inerting that subsequently burned out, returning the hydrogen concentration to safer levels. But, because there are uncertainties in these severe accident cases (source terms and containment modeling), we look to other active safety measures that can eliminate the buildup of the local hydrogen concentrations. One method for improving the situation with regards to local hydrogen accumulation is to supply power to both igniters and fans. With power to the air return fans, mixing in the containment atmosphere is significantly enhanced such that hydrogen burns out in a more uniform manner. However, it must be shown that the amount mixing produced by the fans, while reducing the local buildup of hydrogen, does not also reduce the total amount of hydrogen consumed. For this analysis we use the 26-cell model with igniters, and turn on the fans using the Sequoyah safety trip procedures (containment pressure > 120 kPa, fans on with a ten minute delay).

Shown in Table 6 are controlled hydrogen burn amounts by regions for the cases with and without power to the air return fans. In both cases, the amount of hydrogen consumed is essentially identical, $\sim 2/3$ of the released hydrogen. In the case with fans operating, the burn out is noticeably more uniform. For example, without fans the majority of the hydrogen is consumed in the ice condenser, about 70%. The largest portion of that amount is from burns in the ice bed where there are no igniters, and therefore burning there relies on flame propagation from areas that have igniters. When fans are on, only 40% of the burns occur in the ice condenser; and, of that amount, most of the hydrogen consumed is from burns in the upper plenum where igniters are placed. In general, we may consider this burn pattern, i.e., with fans on, to be a more reliable situation.

The containment pressure for the case with fans on is shown in Figure 46. This profile compares favorably the previously calculated profile with power to the igniters only. When fans are operational, the induced circulation of gas and steam through the ice condenser will increase the amount of ice melting. We compare the ice melt amounts for the cases with and without fan operation in Table 7. Having the fans on results in an additional 25% more ice melt-out at the time of vessel failure, which may be considered a penalty to the subsequent pressure suppression control during ex-vessel energetic events (CCI, etc.).

With the fans on local buildup of hydrogen in the containment is largely eliminated since the likelihood of having inerted regions in the lower containment and ice bed is significantly reduced. With fans, we observed that local increases in hydrogen concentrations in the lower containment and ice bed are reduced. This behavior is evident for the lower containment and ice bed as shown in Figures 47 and 48. However, it is not true that the hydrogen mass distribution is reduced, for instance, in the lower containment by the action of fans. As shown in Table 8, the amount of hydrogen remaining in the lower containment after vessel failure, when power is supplied to both igniters and fans, is approximately twice that amount remaining when power is supplied to only the igniters.

The combination of igniters and fans does reduce the likelihood of local hydrogen concentrations, and provides a more uniform burning of hydrogen throughout the containment. Furthermore, with fans the character of the burns change from those initiated by flame propagation to those mainly ignited by direct ignition. However, the fans do not increase the total amount of hydrogen consumed, and in some regions like the lower compartment, the operation of fans may increase the total amount of hydrogen remaining. Additionally, fan operation provides a only a marginal reduction in containment pressure loading during the accident (up to and including vessel failure). However, allowing the fans to operate does reduce the amount of ice available subsequent to vessel failure by approximately 25%, in the scenario studied. It remains to investigate whether during the post-vessel failure period that the amount of ice remaining at vessel failure will have a noticeable impact on late time containment loading.

6 Summary and Future Work

A short-term station blackout with pump seal leakage scenario has been analyzed using the MELCOR code to determine the potentially severe containment loads that may be produced from a delayed hydrogen burn in the absence of active hydrogen control. The analysis, conducted for the period of time up to and including vessel failure, showed that hydrogen control may be necessary to avoid challenges to the containment. The analysis used detailed descriptions of reactor system sources of water, steam, and hydrogen to the containment as generated by MELCOR code, and reported elsewhere.

Hydrogen control through the supply of power to igniters was studied, as well as the case for power to igniters and fans. Calculations were reported for various containment models where the number of compartments varied from 12 to 38. Results from a 26-cell containment model appeared to give a reasonable representation of the details of hydrogen distribution and controlled burning. The effect of ice bed nodalization and gas/steam bypass pathways were discussed in terms of their impact on hydrogen distributions and hydrogen control.

For a scenario with power to igniters only, it was shown that 1) globally significant hydrogen concentrations can be safely reduced with the potential for a severe delayed

burn avoided, and 2) local hydrogen build-up in the lower containment and ice bed can be mainly eliminated, except for those brief periods when steam injection inerts regions and/or oxygen concentrations are too low to sustain a controlled burn. Fan operation, by mixing the gases in the containment, is shown to help prevent steam inerting in local regions of the ice bed and the lower containment, and to enable a more uniform distribution of burning in the containment. Additionally, the use of fans is shown to cause more igniter initiated burns and less burns in regions where burning must rely on flame propagation. Although the fans help to change the uniformity of the controlled burning, they do not increase the total amount of hydrogen consumed over the case with only the igniters operating, and use of fans can result in more hydrogen (kg) remaining in regions such as the lower containment at the time of vessel failure.

Clearly, this work is at a preliminary stage. We have yet to perform required uncertainty studies of hydrogen burn parameters such as flame propagation limits, etc. Most importantly, source term uncertainty results still need to be folded into the analysis, and other scenarios included. Additionally, this initial effort focused only on the period of the accident up to and including vessel failure. While this period was shown to produce potentially damaging containment pressure loads (delayed burns), it remains to investigate the long-term accidents that include ex-vessel phenomena such as core concrete interaction (time out to 24 hours).

Table 1. Reference MELCOR containment models for the Sequoyah plant.		
CVH Nos.*		Location
26-cell	12-cell	
1	1	Cavity
2-5	2-3	Steam Gen. Doghouses
6	6	Upper Reactor Space
7	7	Pressurizer Doghouse
8-10	8-9	Lower Containment (Inside Crane Wall)
11-13	11	Lower Annulus (Between Crane Wall and Shell)
14-17	14	Lower Plenum
18-21	18	Ice bed
22-23	22	Upper Plenum
24-25	24	Upper Dome
26		Lower Dome & Operating Floor

* note the CVH package of MELCOR does not require that compartments (cells) be sequenced in any order.

Table 2. Revisions for the Reference MELCOR containment models in preparation for Hydrogen distribution and deflagration analysis.

Revision topic	26-cell	12-cell
Ice mass increased to 100% FSAR mass reported	Correctly model	Original model included ~ 25% (input error)
Ice bed flow area adjusted to total amount	Correctly model	Original model set to 25% of area
Heat of reaction and upper temperature bound for ice melting (degas input) changed to reflect observations from Waltz Mill long-term test results	Applies to both models	
Refueling drain elevations set at refueling floor level	Applies to both models	
Include deck bypass flow area (NUREG 5586)	Previously commented out	
Redirection of RCS injection sources to appropriate lower containment compartments	Applies to both models	
Add input for possible latching of lower plenum doors if hinge crushing assumed	Option for crushing not assumed for these severe accident scenarios in general; however, option may be used during deflagration condition in subsequent calculations	
External file reads for RCS sources	Applies to both models	
Igniter locations set to Sequoyah description (SSER 6)	Applies to both models	
Lower containment and refueling canal flooding profile added (required for flooding of refueling drains and cavity overflow at correct accumulated water volume)	Applies to both models	
Fan trip input revision	Functional delay added	

Table 3. Ignition and propagation limits for deflagrations.

Limits	X (H ₂)*	X (O ₂)	X (steam)
Ignition	≥ 0.05	≥ 0.05	≤ 0.55
Upward propagation	≥ 0.041	≥ 0.05	≤ 0.55
Horizontal propagation	≥ 0.06	≥ 0.05	≤ 0.55
Downward propagation	≥ 0.09	≥ 0.05	≤ 0.55

Table 4. Igniter locations used in the analysis of the Sequoyah plant.

Location	Igniters
Cavity	No
Steam Gen. Doghouses	Yes
Upper Reactor Space	Yes
Pressurizer Doghouse	Yes
Lower Containment (Inside Crane Wall)	Yes
Lower Annulus (Between Crane Wall and Shell)	Yes
Lower Plenum	No
Ice bed	No
Upper Plenum	Yes
Upper Dome	Yes
Lower Dome & Operating Floor	Yes

Table 5. Hydrogen consumed in containment for period up to and including vessel breach (power to igniters only)*

Location	Hydrogen consumed (kg)	
	26-cell model	38-cell model**
Lower containment	100	55
Ice condenser	212	249
Ice bed	161	154
Upper plenum	41	69
Lower plenum	10	26
Upper containment	8	18
Total	320	322

* Total hydrogen released to containment up to and including vessel breach is 475 kg.

** Identical to 26-cell model except for the addition vertical segmentation of the ice bed.

Table 6. Hydrogen consumed in containment for period up to and including vessel breach (26-cell containment model)*

Location	Hydrogen consumed (kg)	
	Igniters only	Igniters and fans
Lower containment	100	150
Ice condenser	212	124
Ice bed	161	46
Upper plenum	41	72
Lower plenum	10	6
Upper containment	8	52
Total	320	325

* Total hydrogen released to containment up to and including vessel breach is 475 kg.

Table 7. Amount of ice melt for the station blackout accident with pump seal leakage.

Scenario	Ice melt (kg)	Percentage of total ice mass*
No power (no burns)	6.02e5	55%
Power to igniters	6.16e5	56%
Power to igniters and fans	8.8e5	80%

* Initial mass of ice in ice condenser is 1.1e6 kg

Table 8. Amount of hydrogen remaining in the containment at time of vessel failure (Short-term station blackout with pump seal leakage).*

Location	No burns kg	Igniters kg	Igniters and fans kg
Lower containment	47	19	36
Ice condenser	140	40	28
Upper containment	289	94	86

* 26-cell containment model

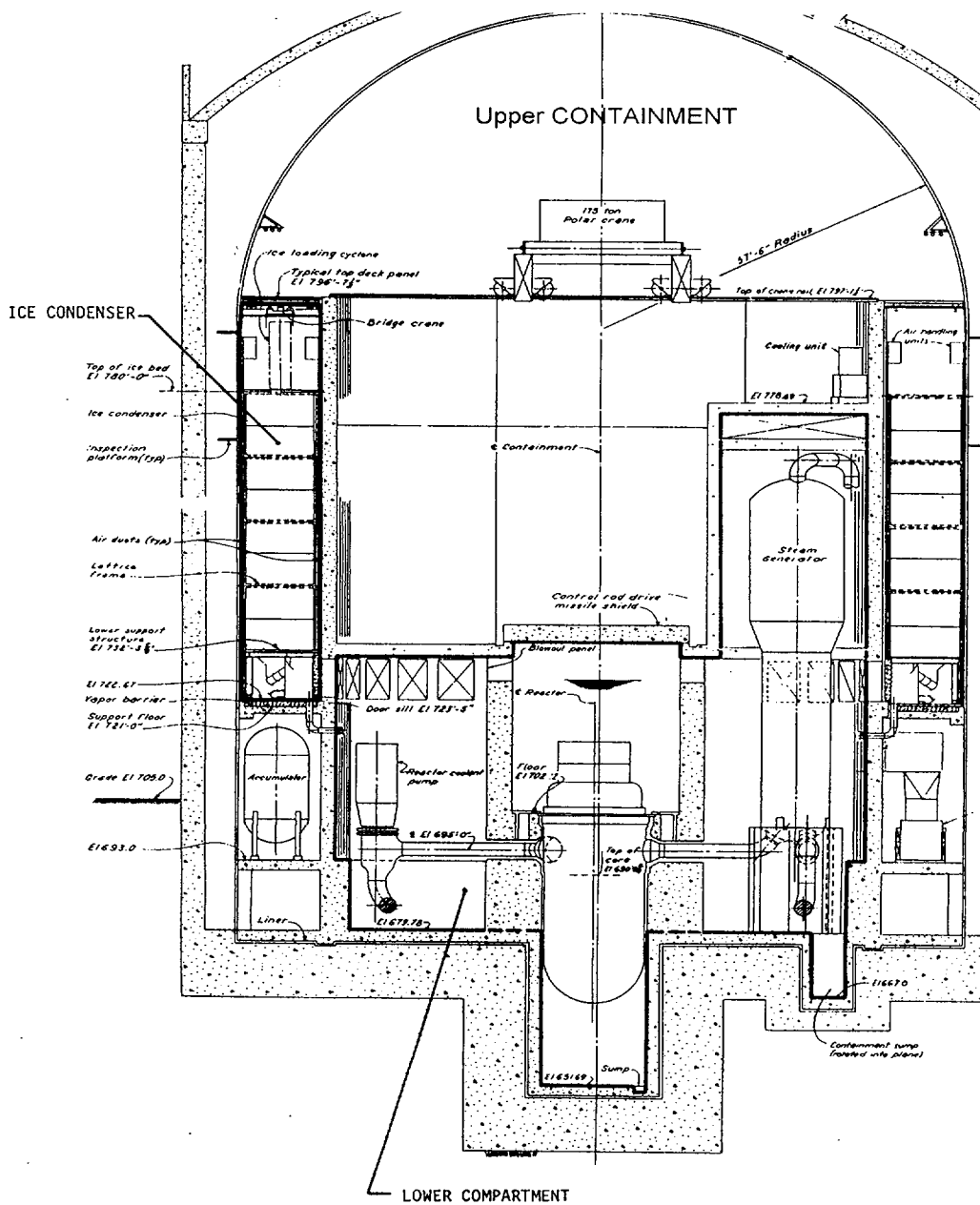
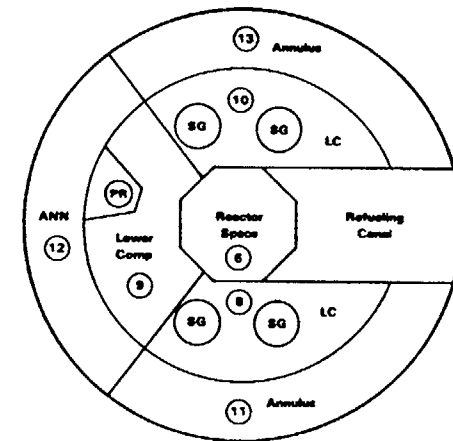
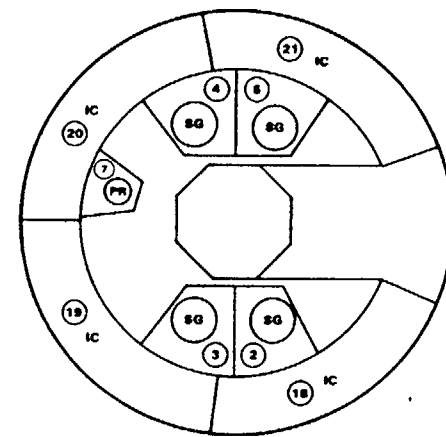
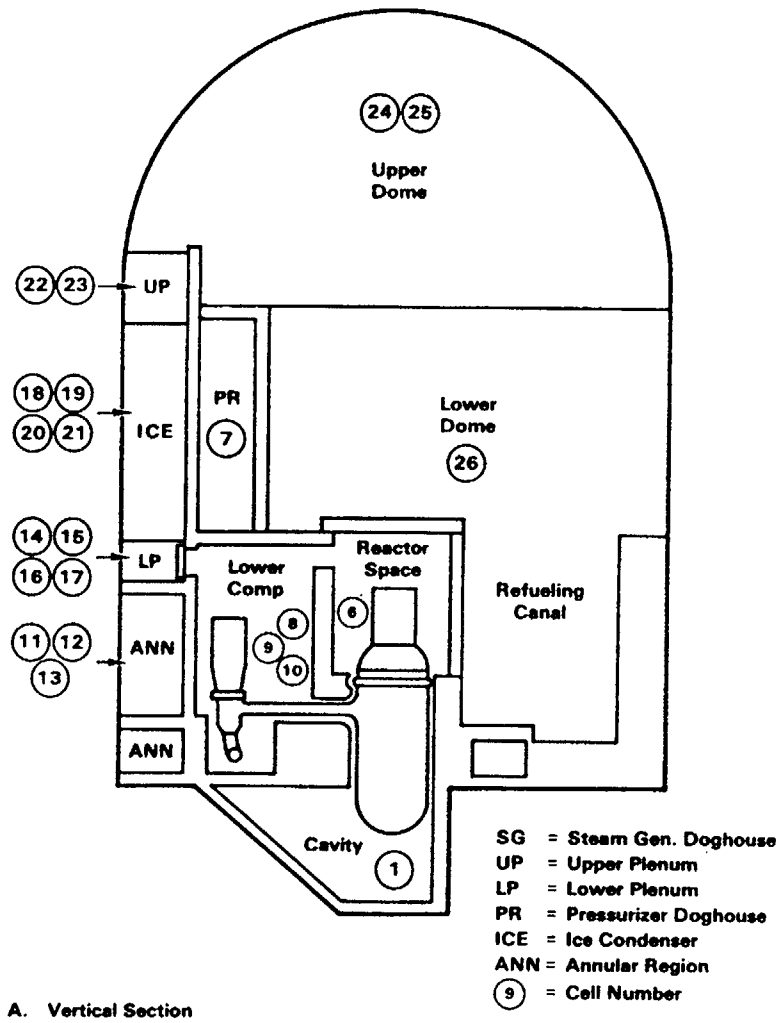


Figure 1 Sequoyah containment drawing [Sequoyah FSAR].

Figure 2 Sketch of Sequoyah containment nodalization for the 26-cell MELCOR containment model.



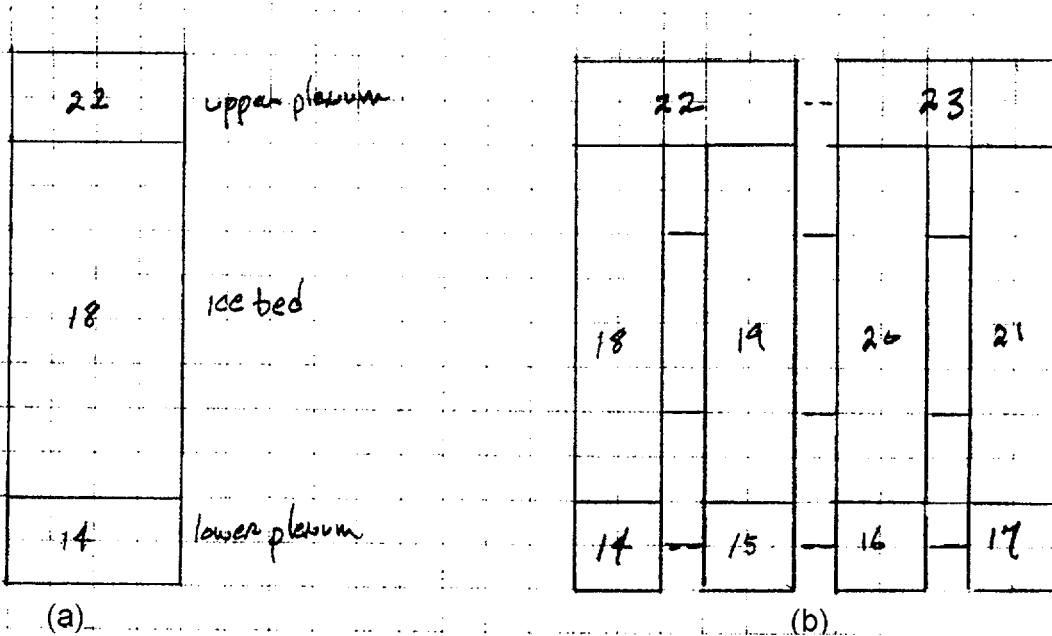


Figure 3 Ice bed nodalizations for the 12-cell (a) and 26-cell (b) MELCOR containment models.

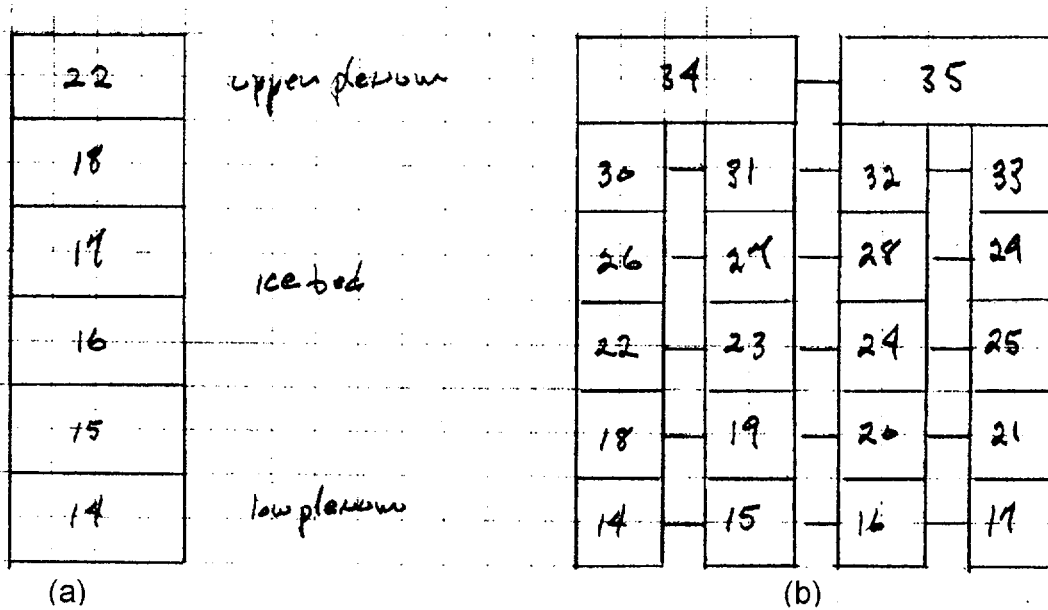


Figure 4 Ice bed nodalizations for the 15-cell (a) and 38-cell (b) MELCOR containment models.

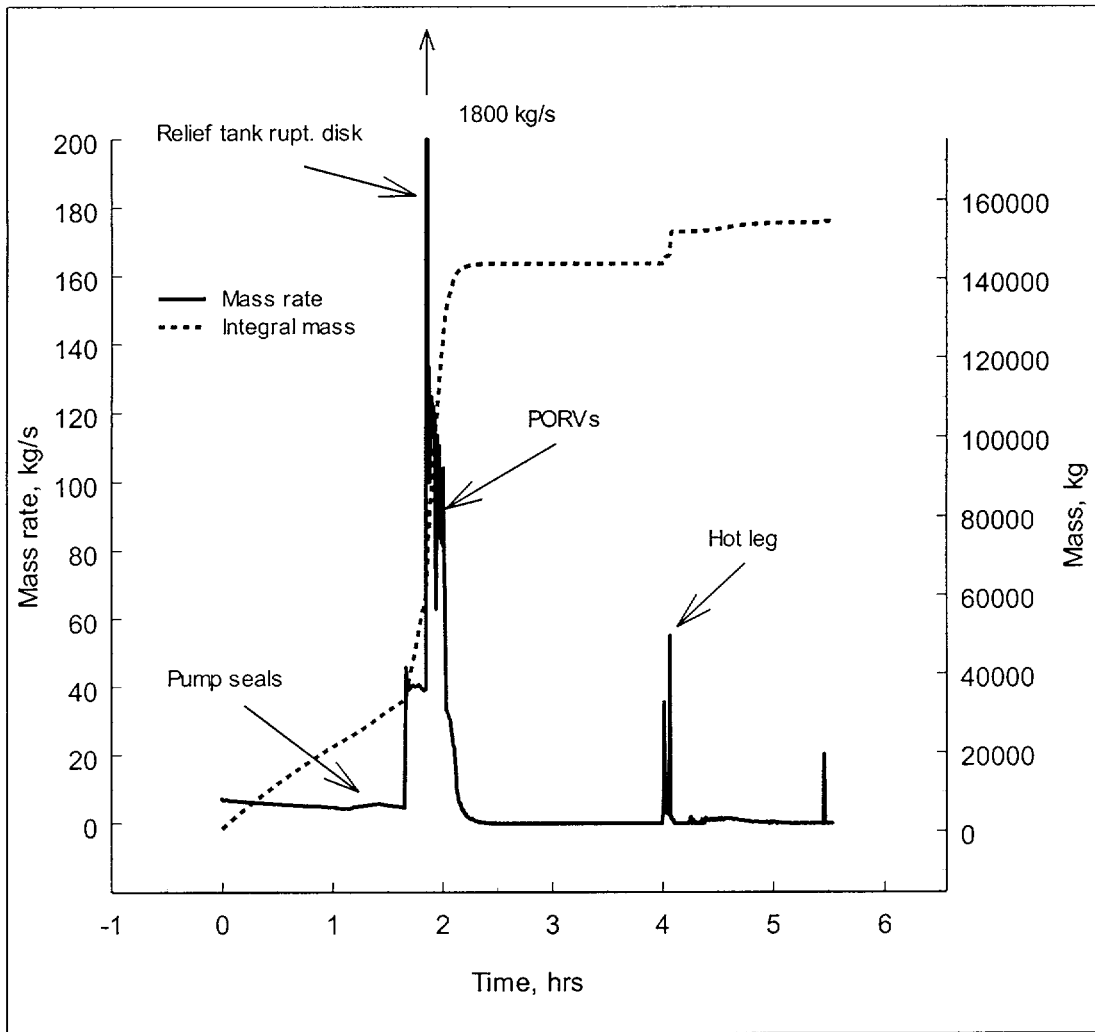


Figure 5 Liquid water source to lower containment for Sequoyah, STSBO-L1.

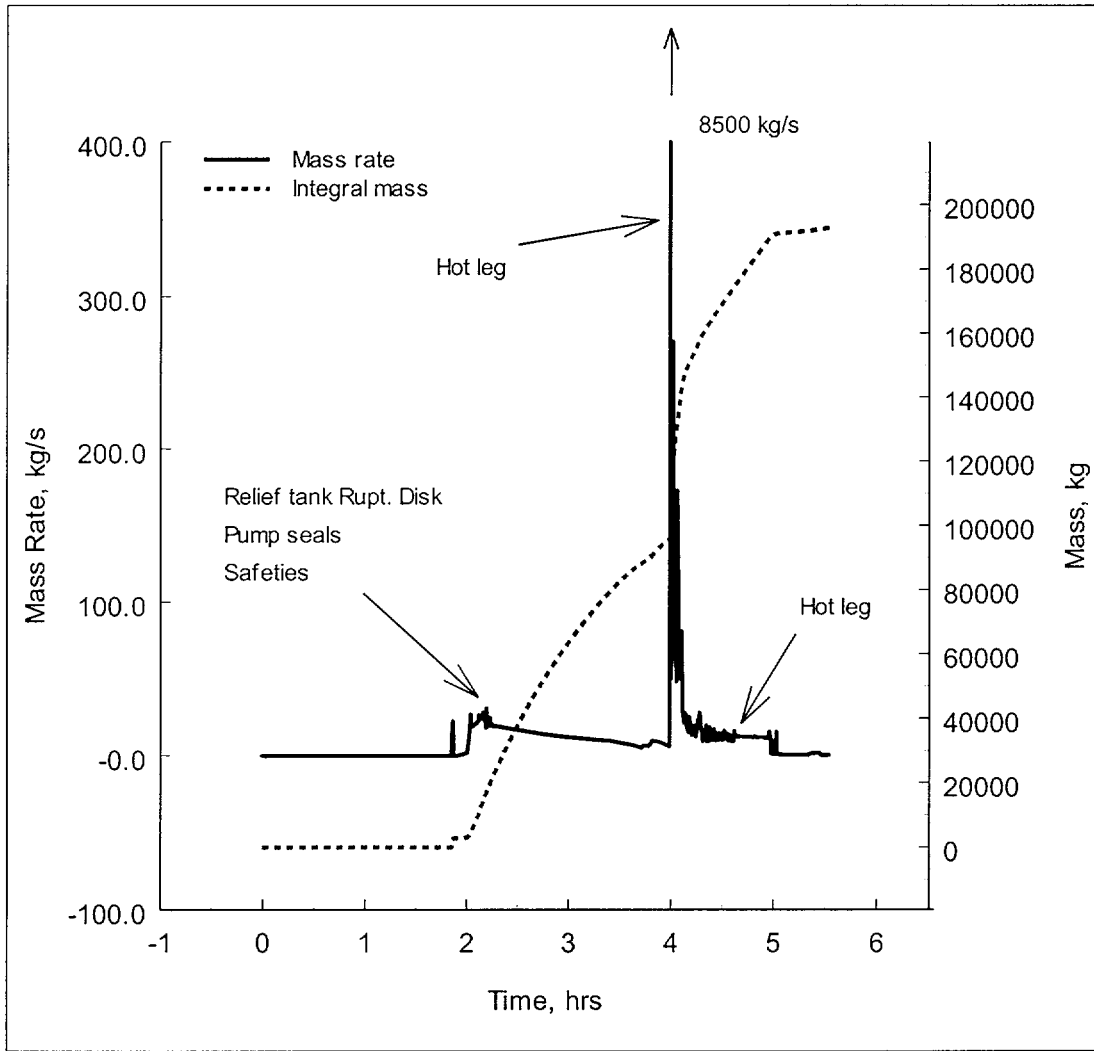


Figure 6 Steam source to lower containment for Sequoyah, STSBO-L1.

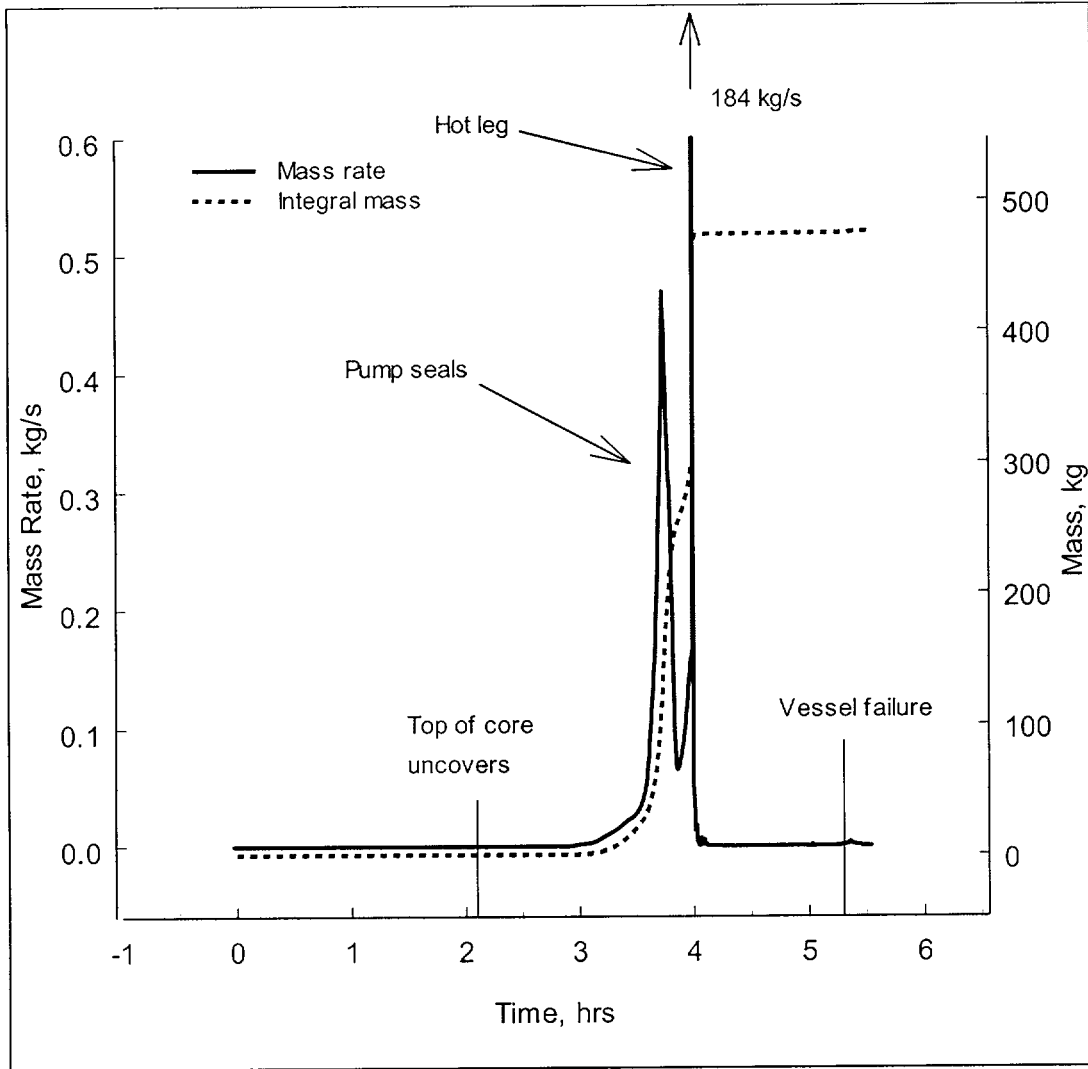


Figure 7 Hydrogen source to lower containment for Sequoyah, STSBO-L1.

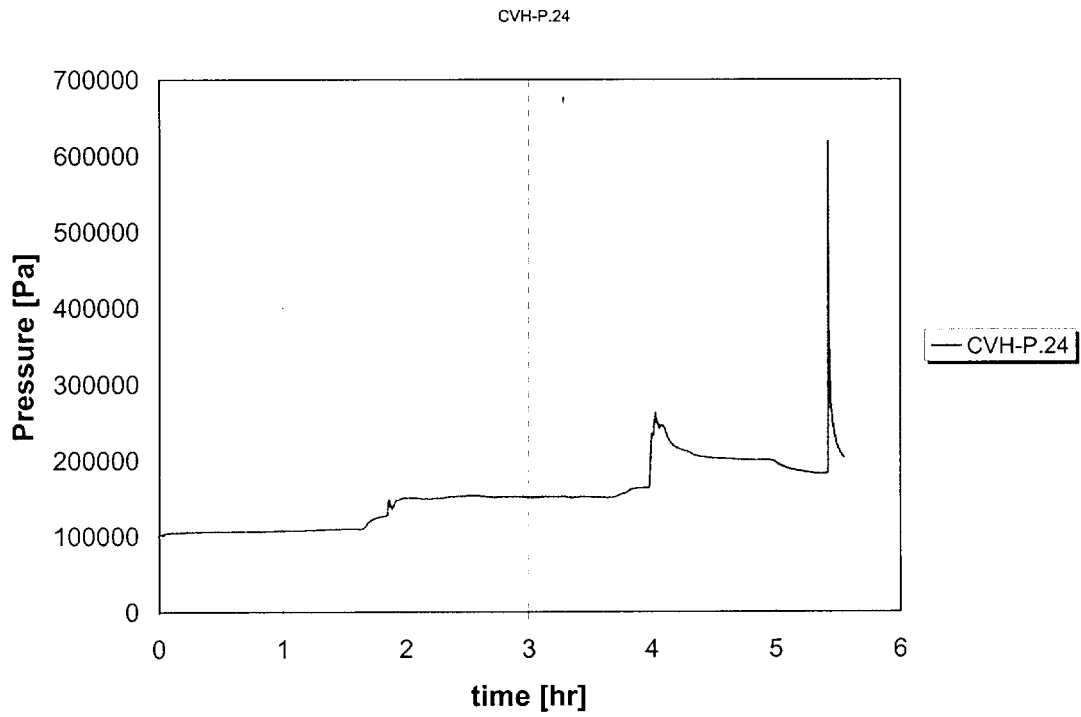


Figure 8 Upper containment pressure history (26-cell model) for delayed burn at VB.

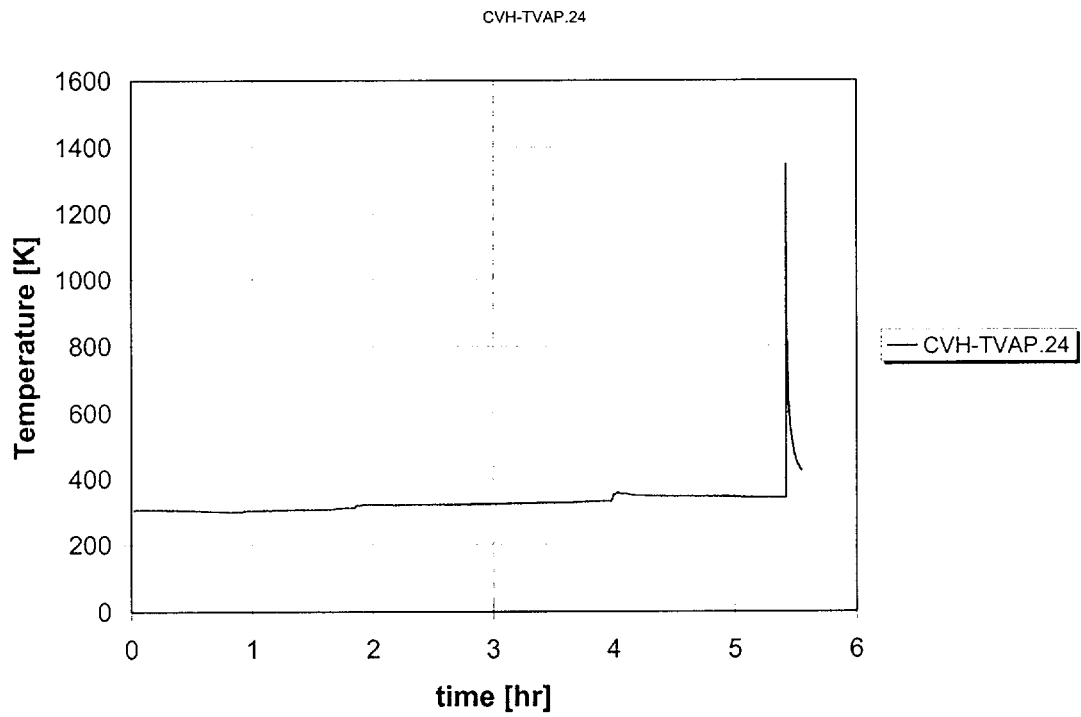


Figure 9 Upper containment temperature history (26-cell model) for delayed burn at VB.

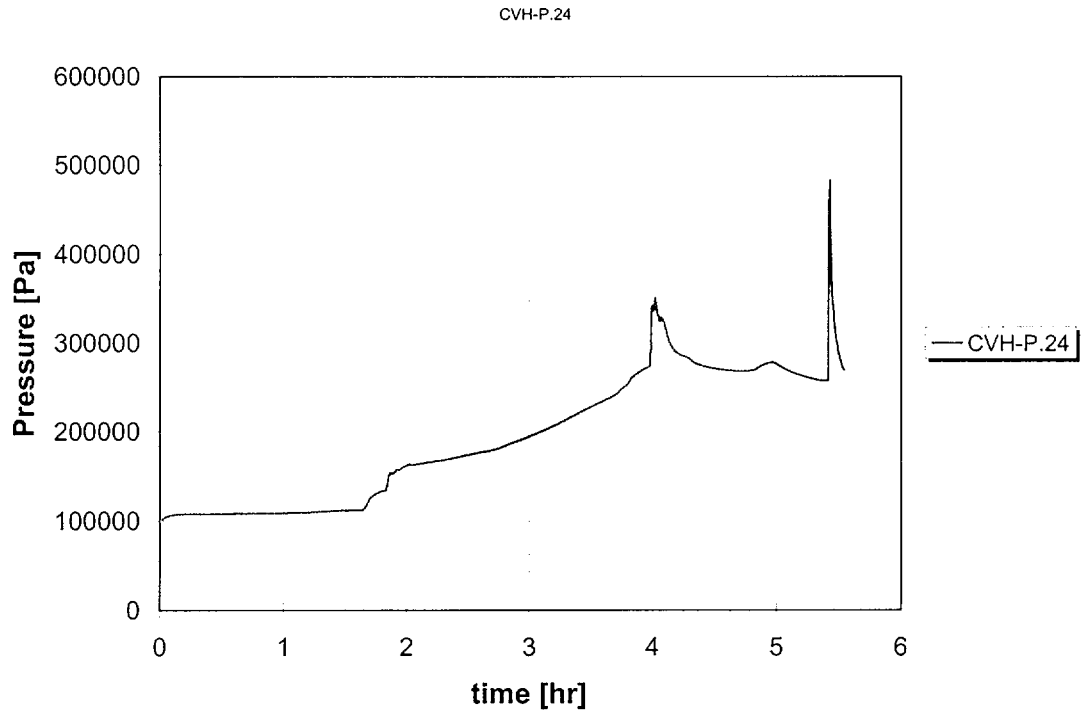


Figure 10 Upper containment pressure history (15-cell model) for delayed burn at VB.

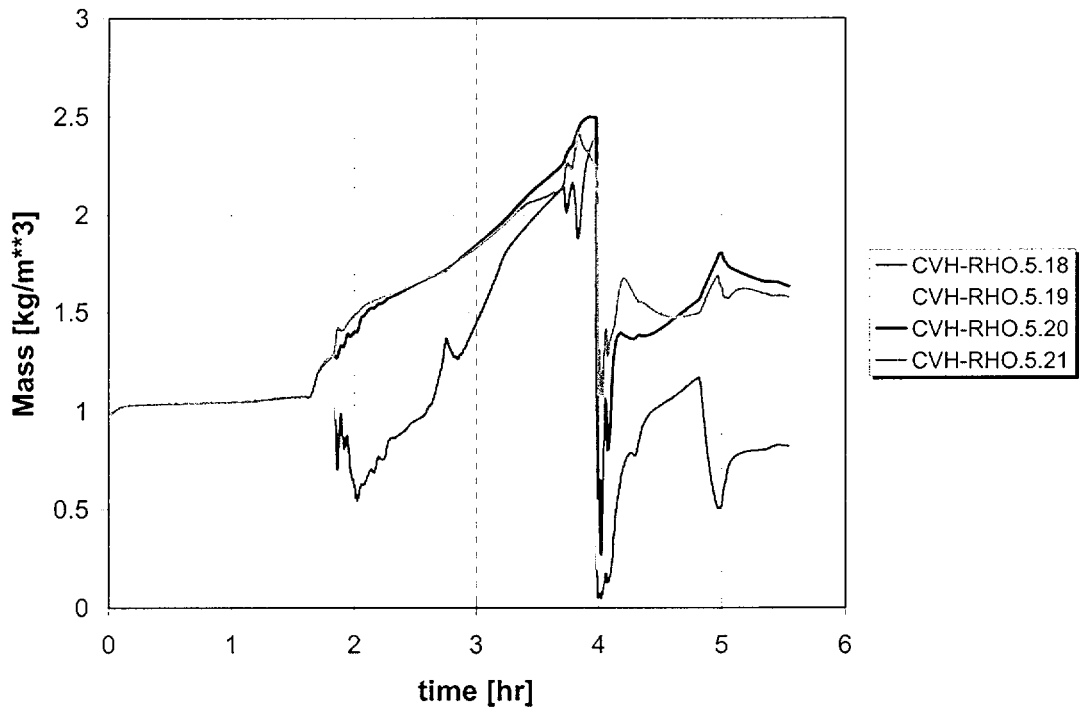


Figure 11 Air density ($\rho_{0.5}$ = nitrogen) in the ice bed for the 15-cell containment model (see Figure 4a).

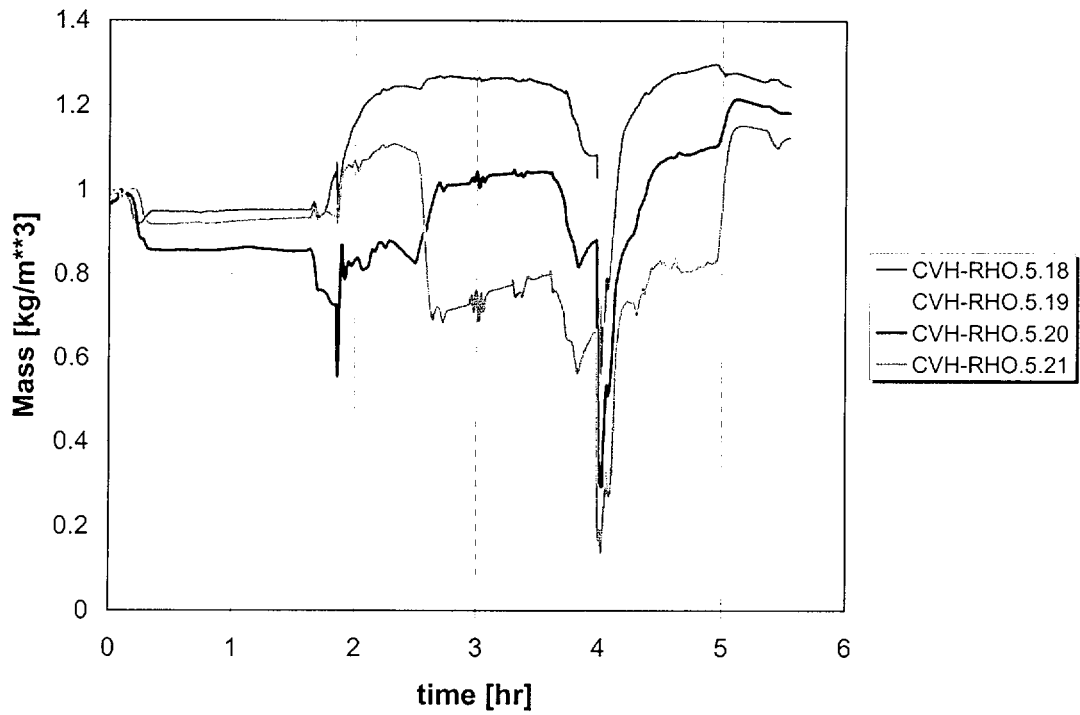


Figure 12 Air density (rho.5 = nitrogen) in the ice bed for the 26-cell containment model (see Figure 3b).

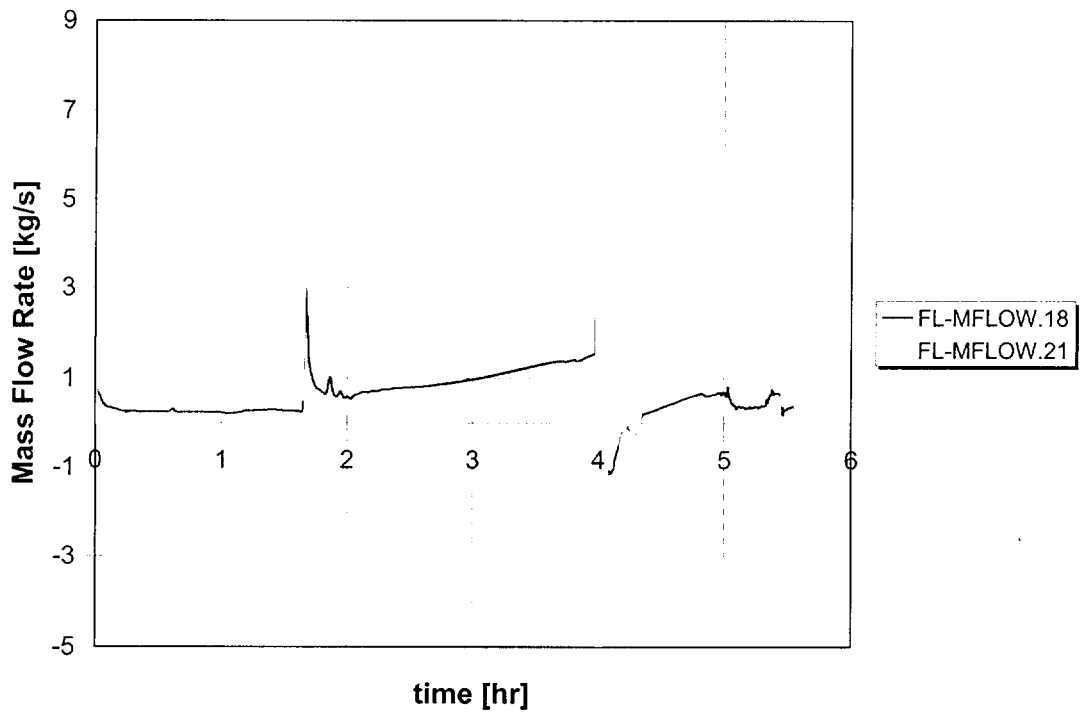


Figure 13 Bypass flow for the 15-cell model (positive flow is from lower to upper containment).

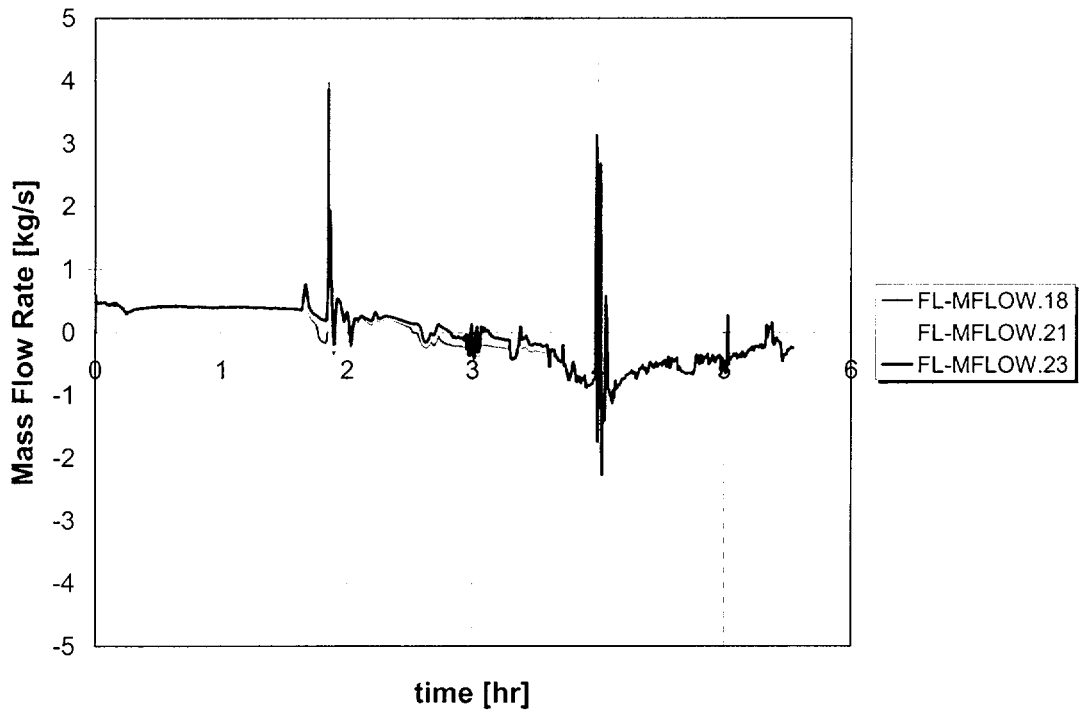


Figure 14 Bypass flow for the 26-cell model (positive flow is from lower to upper containment).

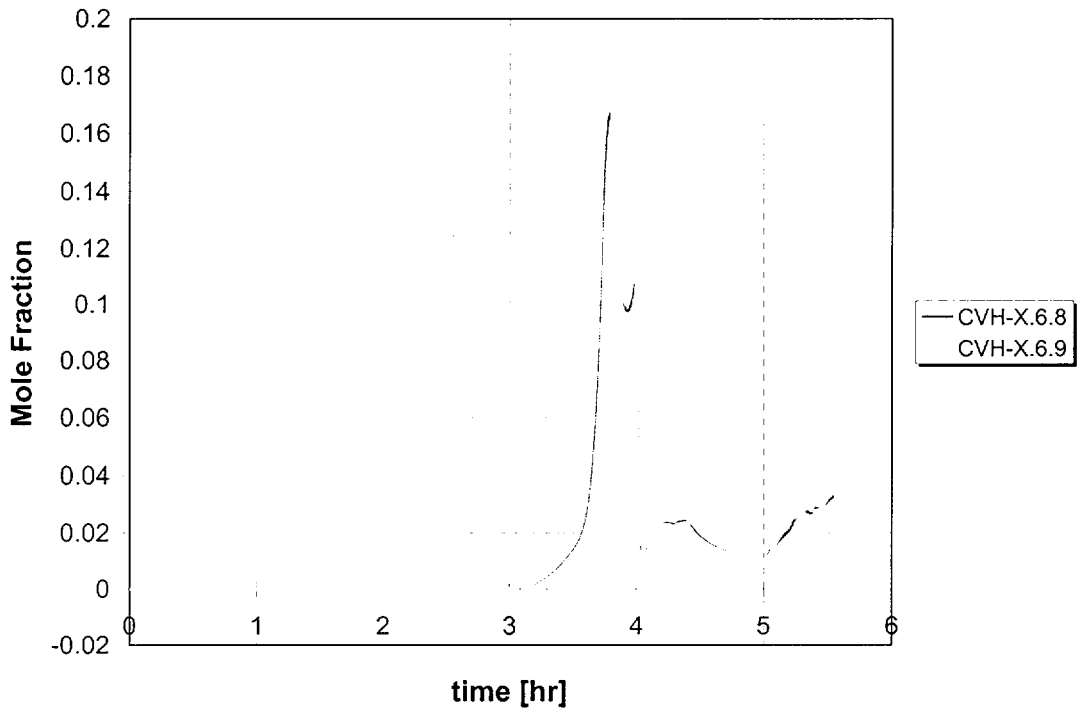


Figure 15 Lower containment hydrogen concentrations for 12-cell model.

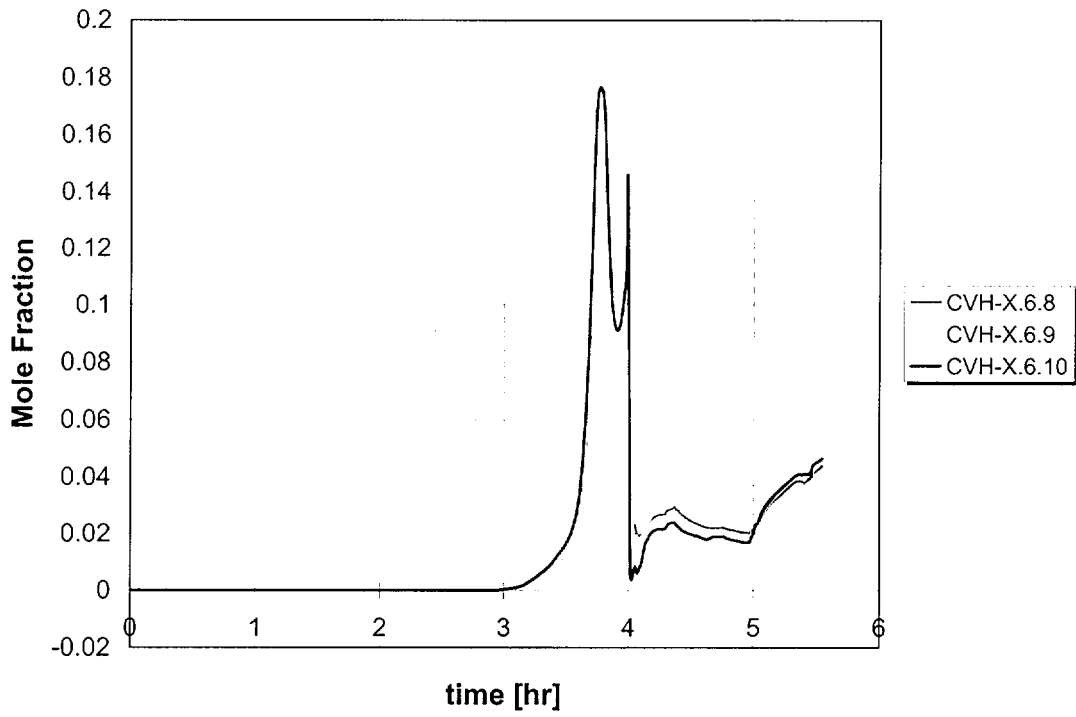


Figure 16 Lower containment hydrogen concentration for 26-cell model.

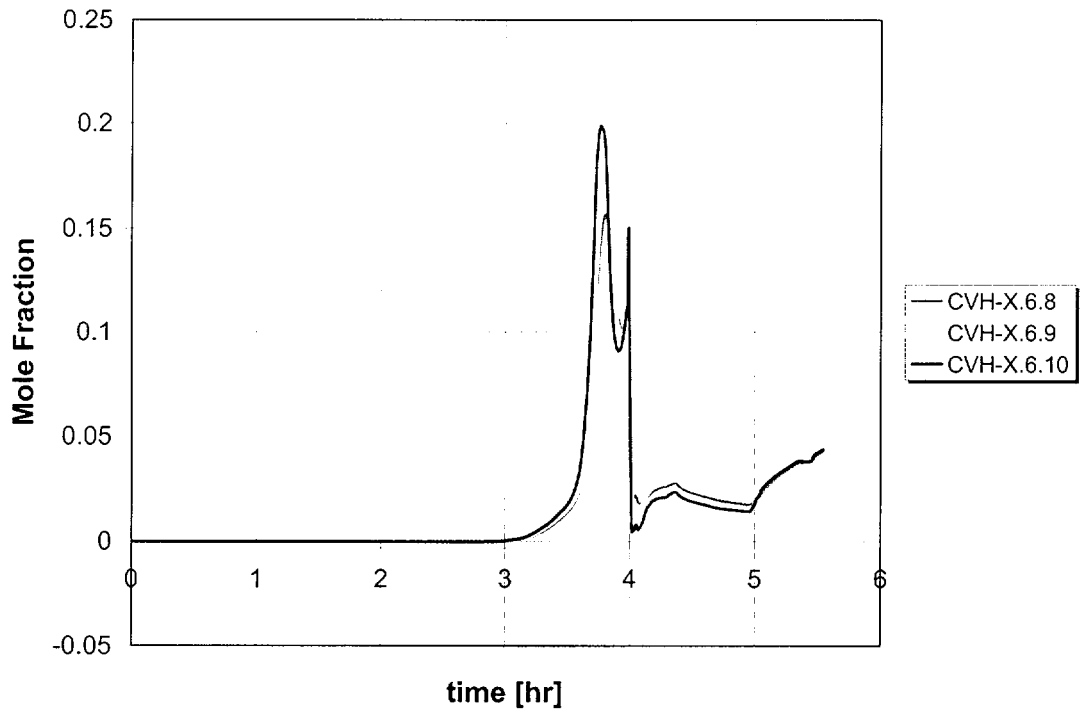


Figure 17 Lower containment hydrogen concentration for the 38-cell model.

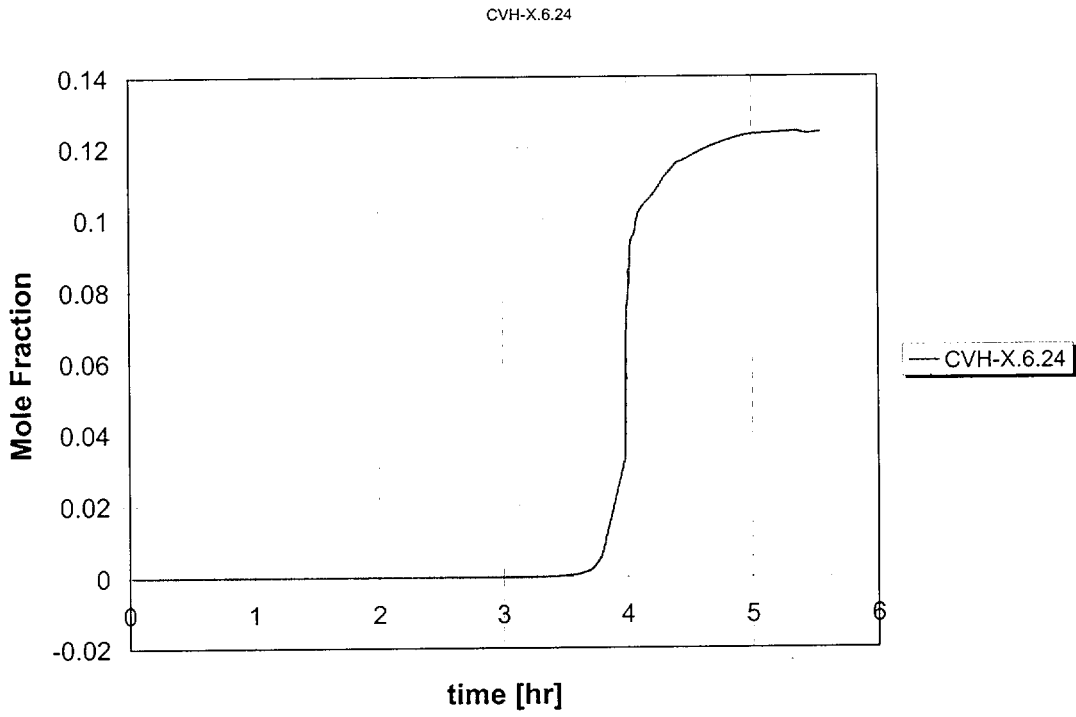


Figure 18 Upper containment hydrogen concentration for the 12-cell model.

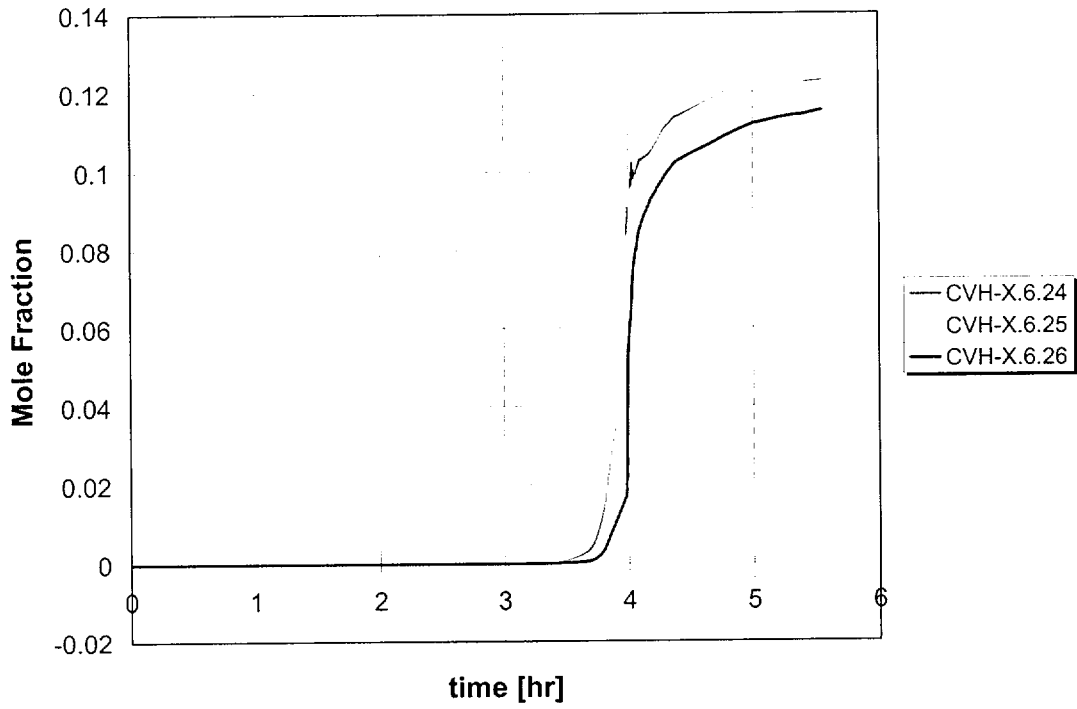


Figure 19 Upper containment hydrogen concentration for the 26-cell model.

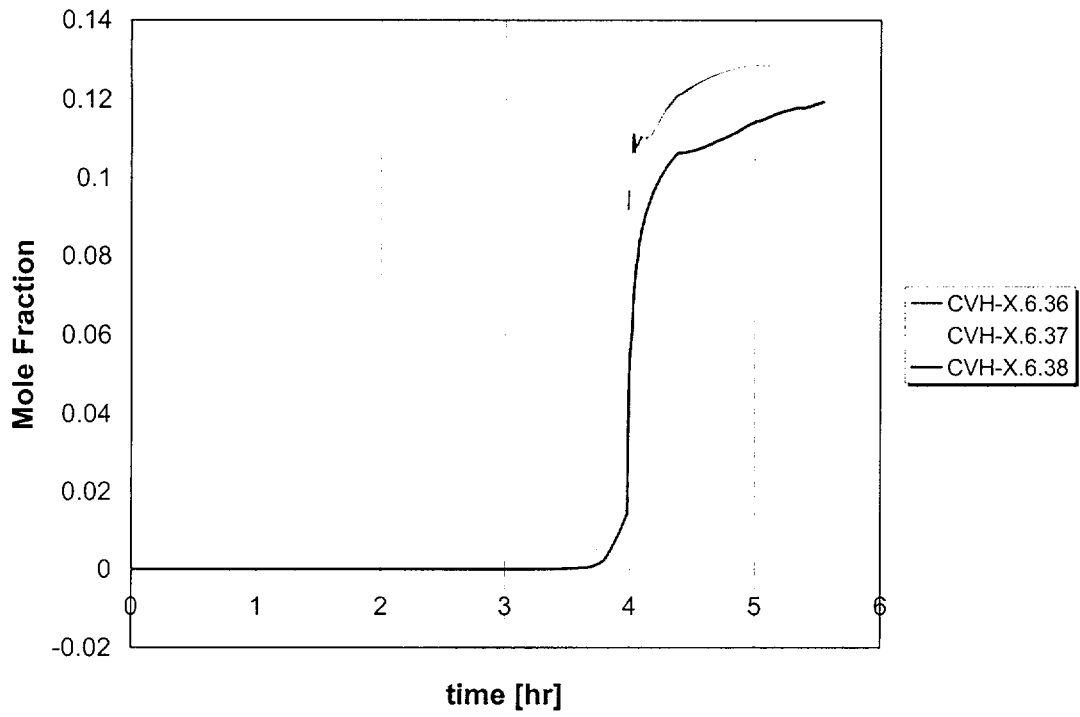


Figure 20 Upper containment hydrogen concentration for the 38-cell model.

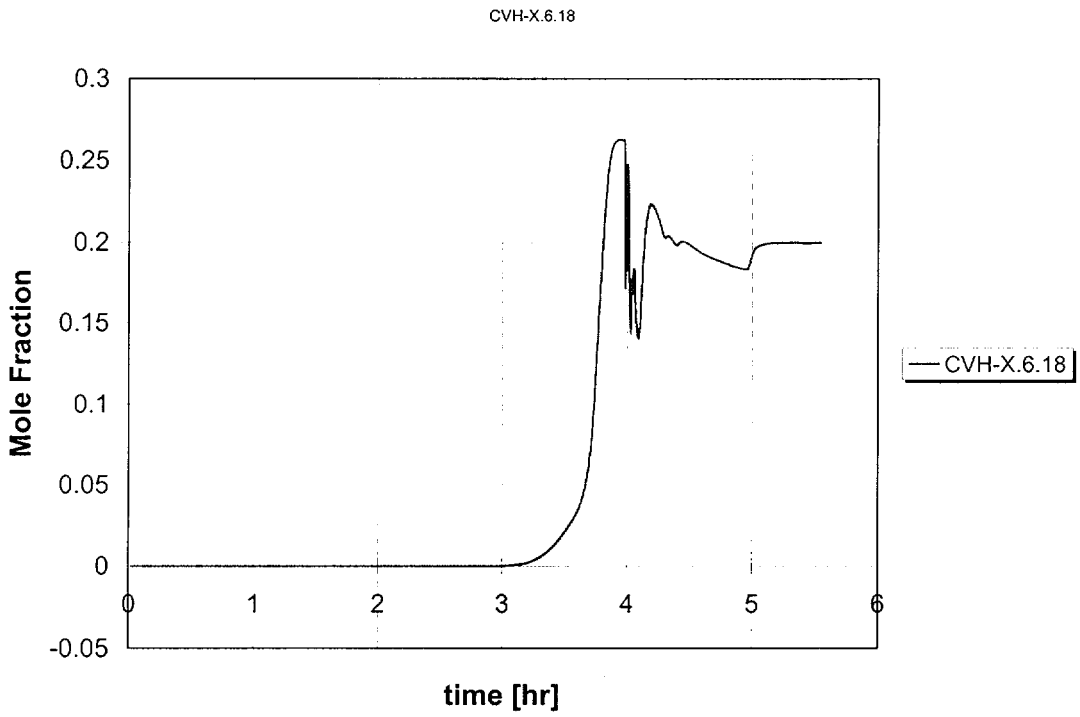


Figure 21 Ice bed hydrogen concentration for the 12-cell model.

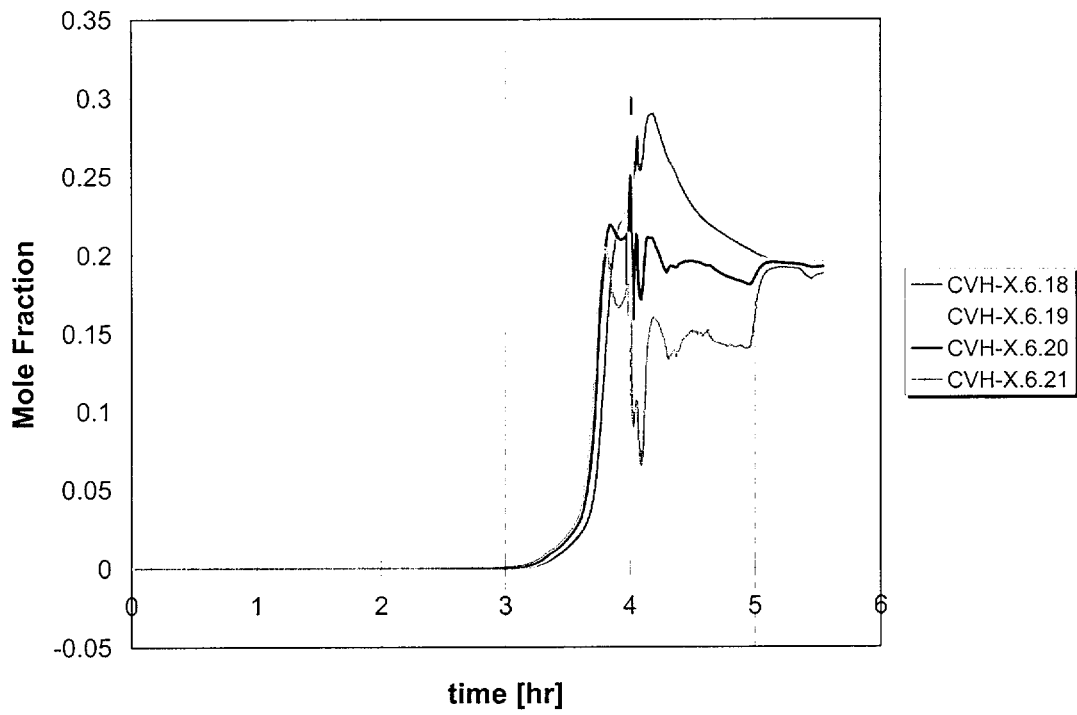


Figure 22 Ice bed hydrogen concentration for the 26-cell model.

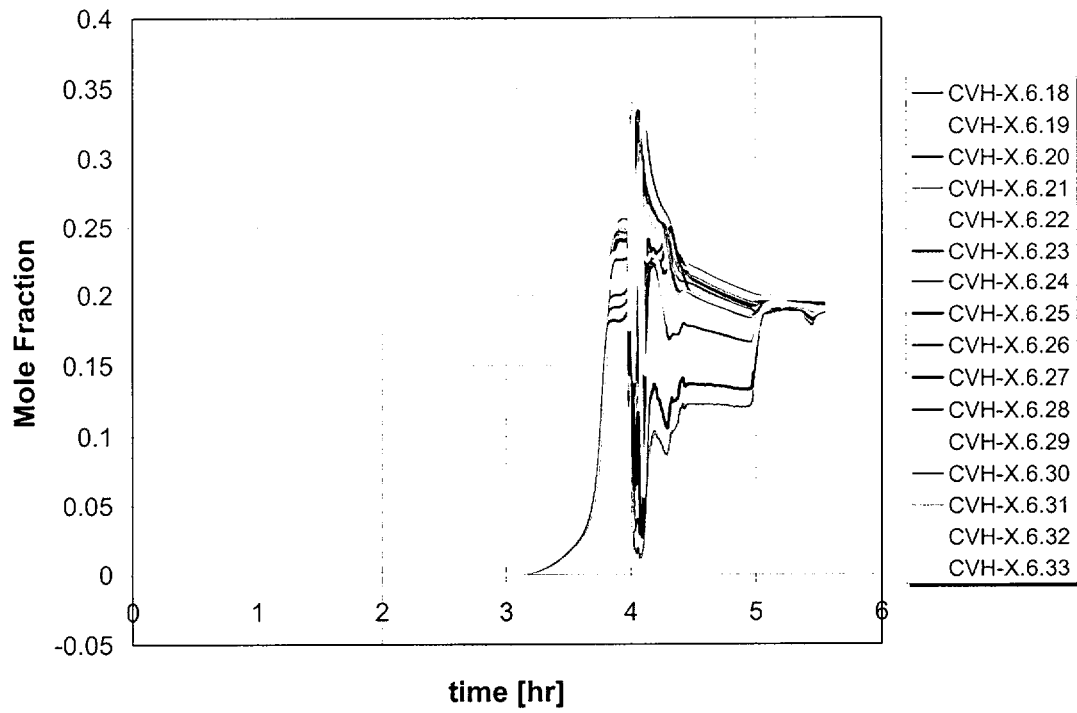


Figure 23 Ice bed hydrogen concentration for the 38-cell model.

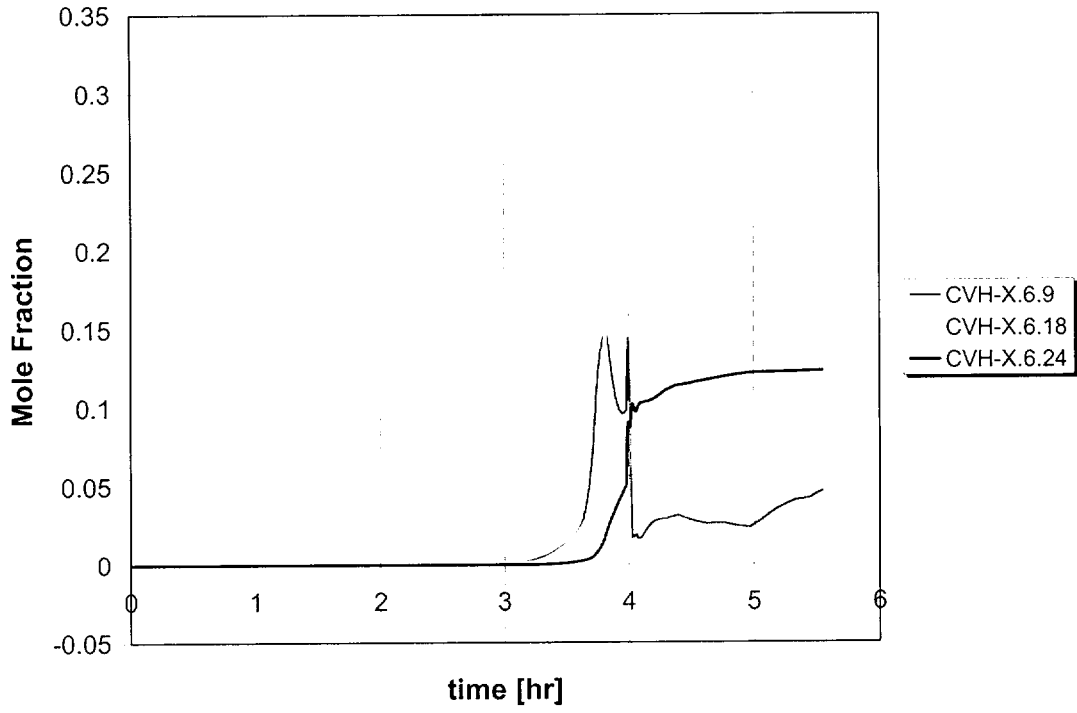


Figure 24 Hydrogen concentration in the containment using the 26-cell reference model.

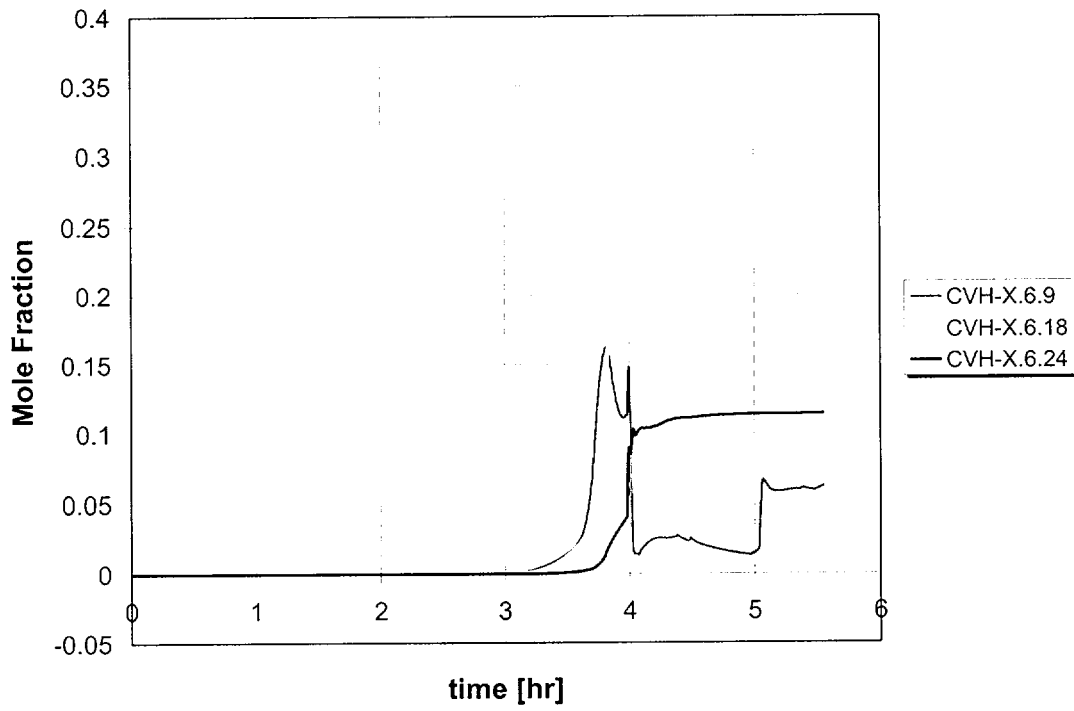


Figure 25 Hydrogen concentration in the containment with the bypass flow area reduced by factor of ten.

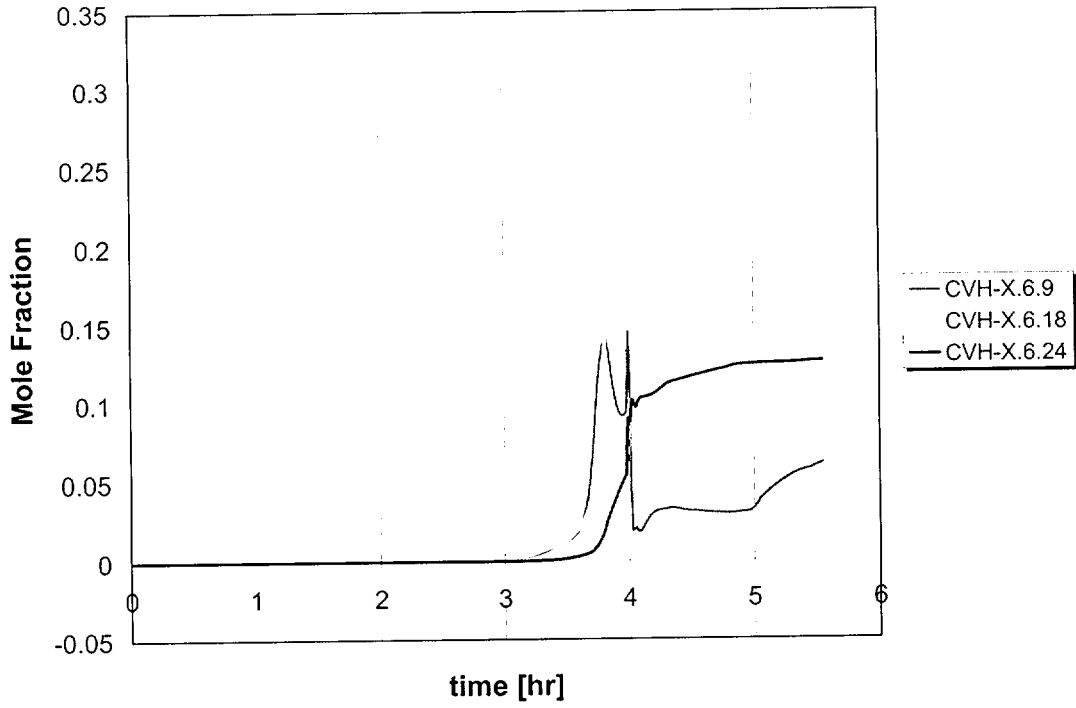


Figure 26 Hydrogen concentration in the containment with the bypass flow elevation reduced to 13 meters.

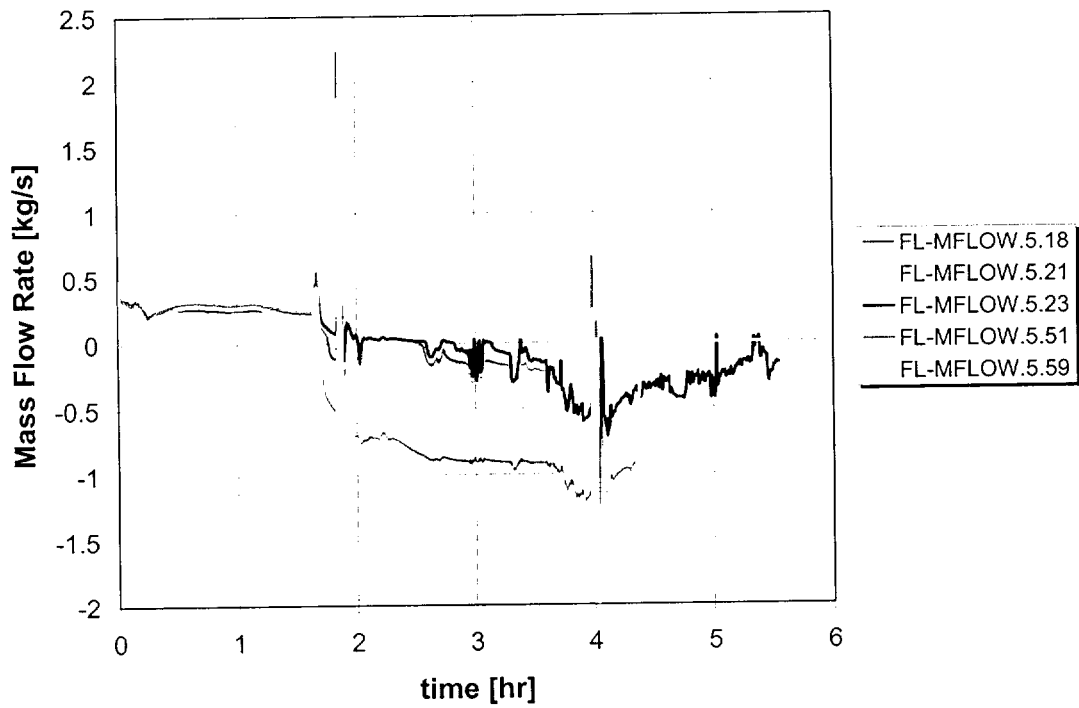


Figure 27 Bypass (18-23) and drain air flows (51-59) for the reference 26-cell model.

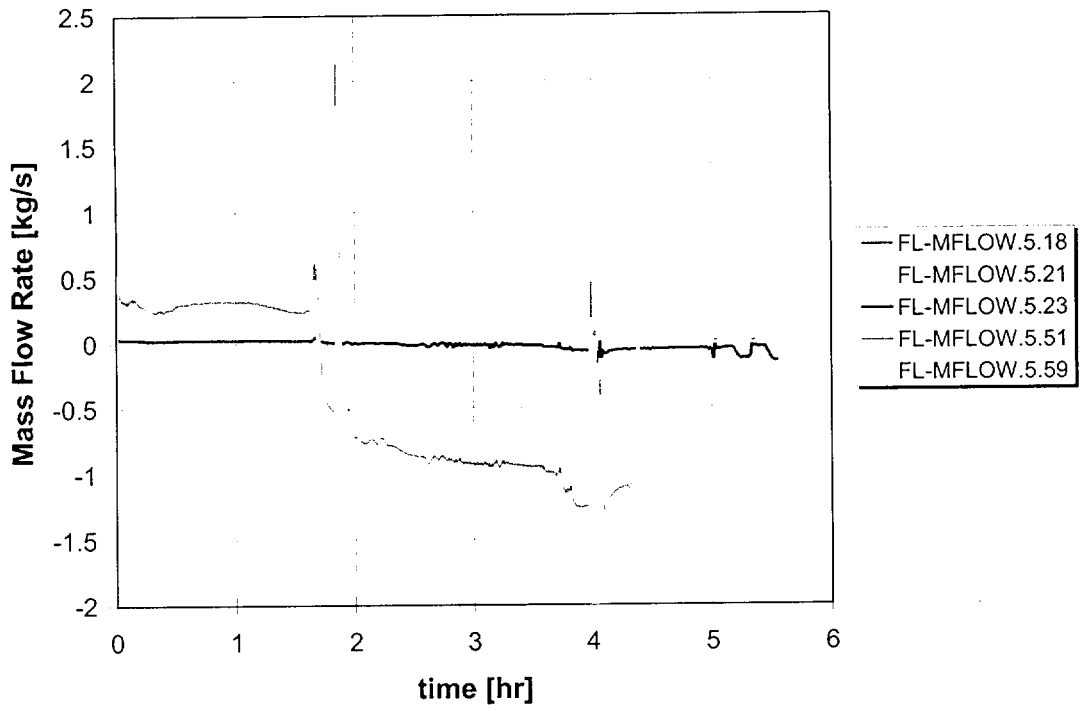


Figure 28 Bypass (18-23) and drain air flows (51-59) for case with bypass flow area reduced by factor of ten.

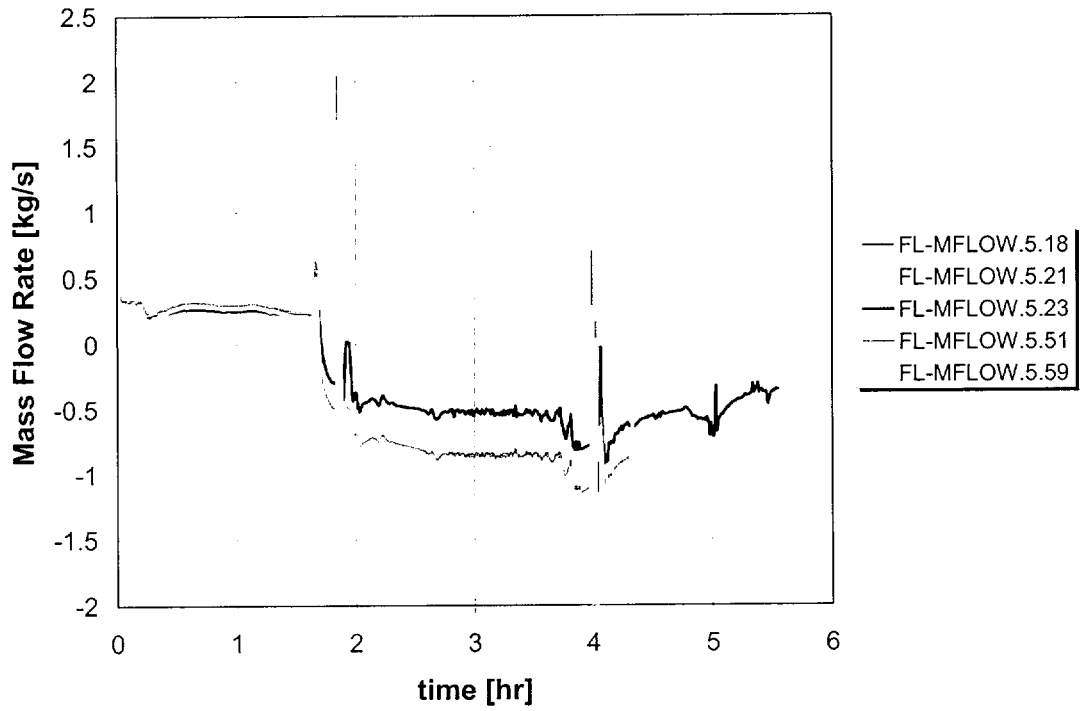


Figure 29 Bypass (18-23) and drain air flows (51-59) for case with bypass flow elevation changed from 20 to 13 meters.

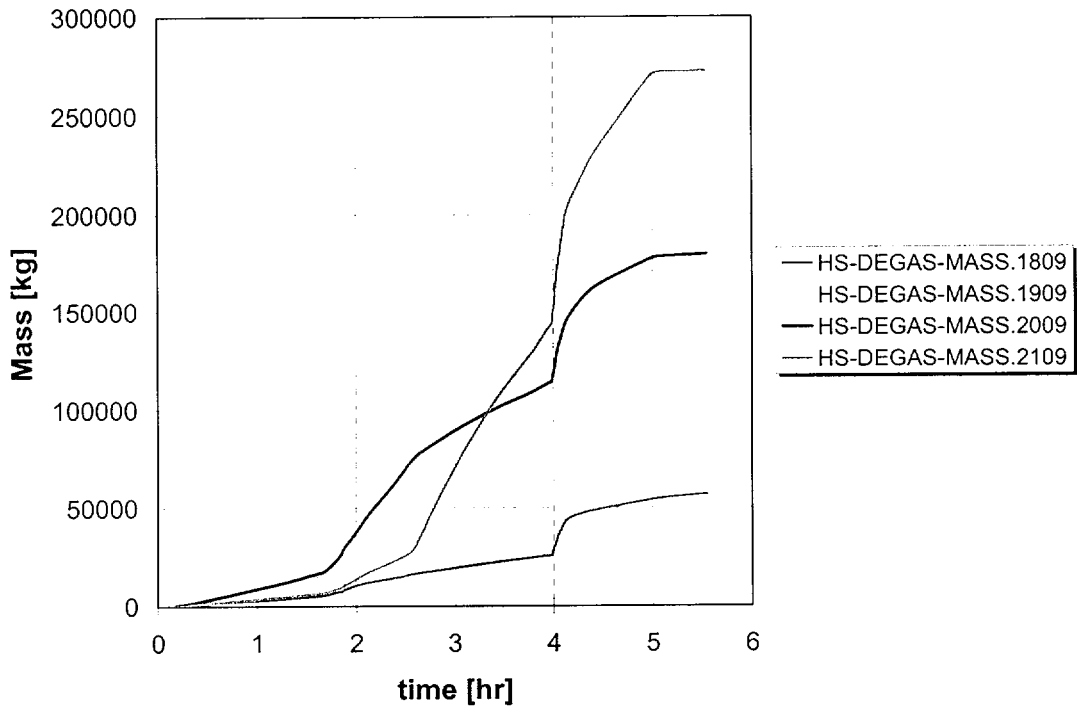


Figure 30 Ice melt amount for the ice bed compartments 18-21 in the 26-cell containment model.

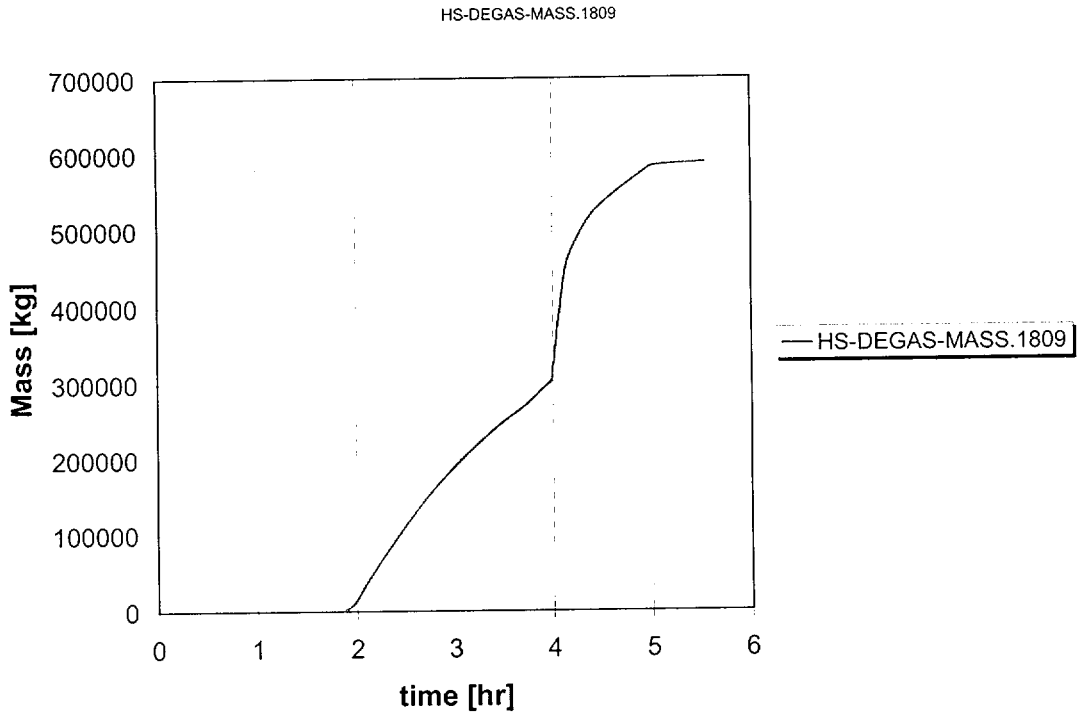


Figure 31 Ice melt amount for the ice bed compartment (18) in the 12-cell containment model.

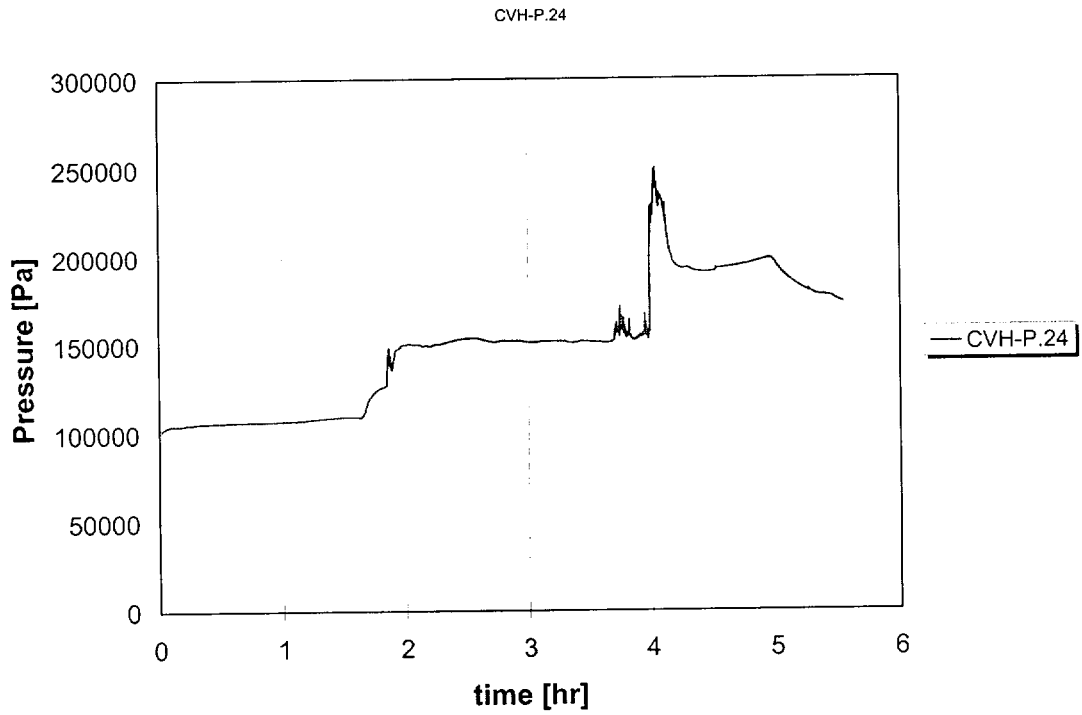


Figure 32 Containment pressure for controlled burning, power to igniters only (26-cell model).

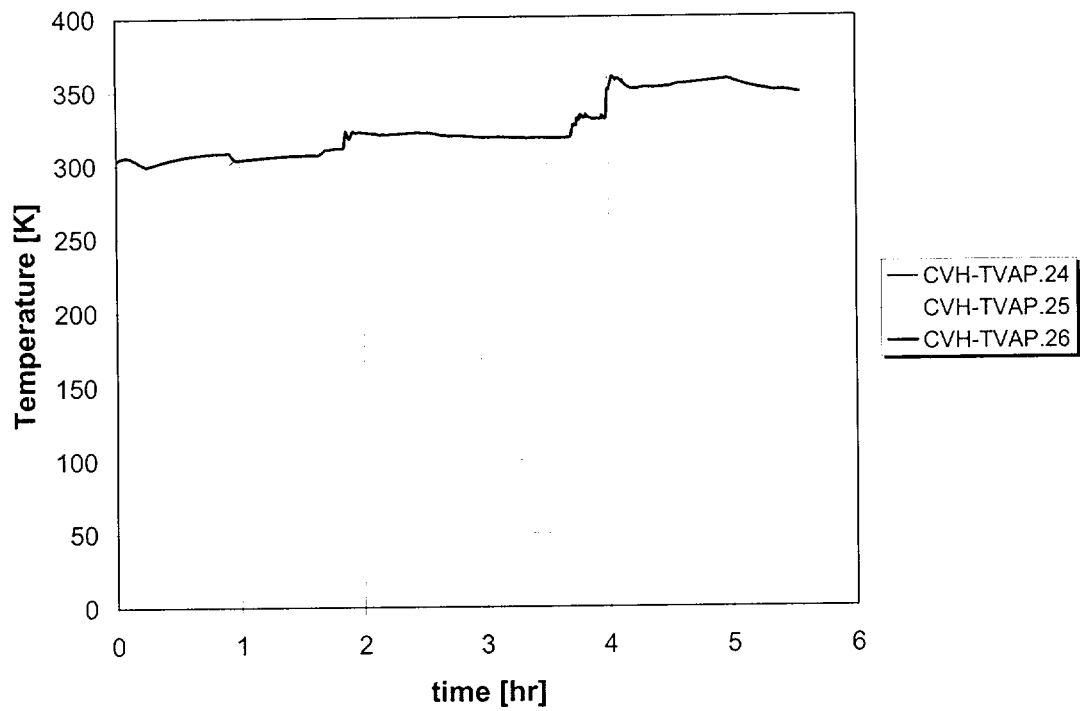


Figure 33 Upper containment temperature, power to igniters only (26-cell model).

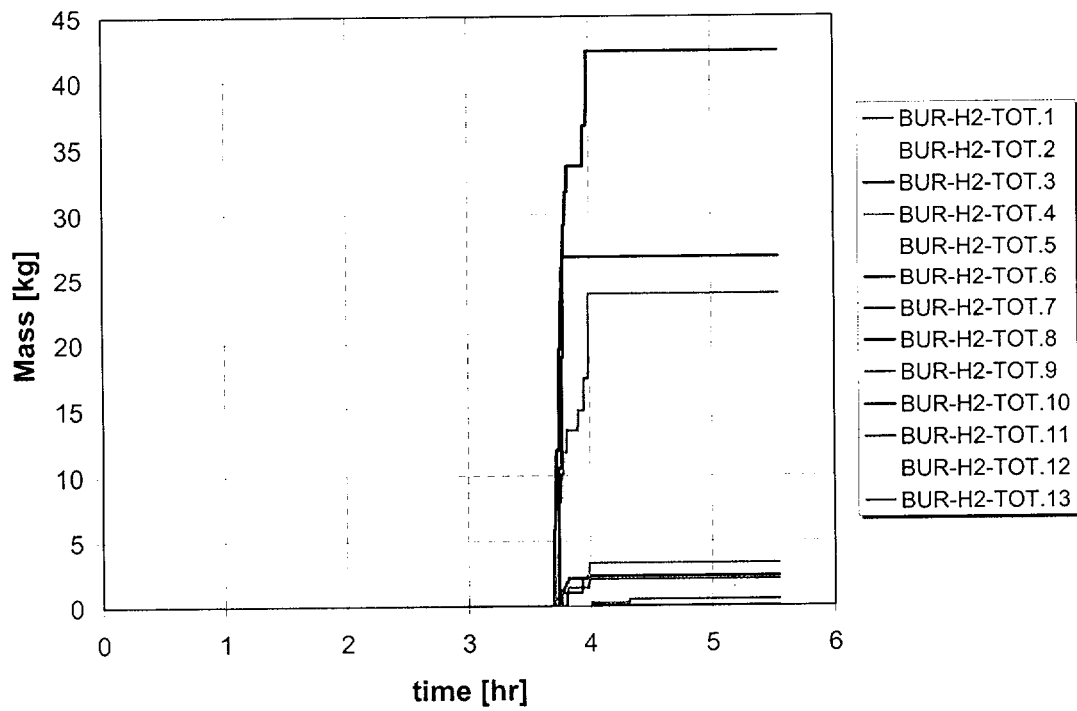


Figure 34 Lower containment hydrogen burned, power to igniters only (26-cell model).

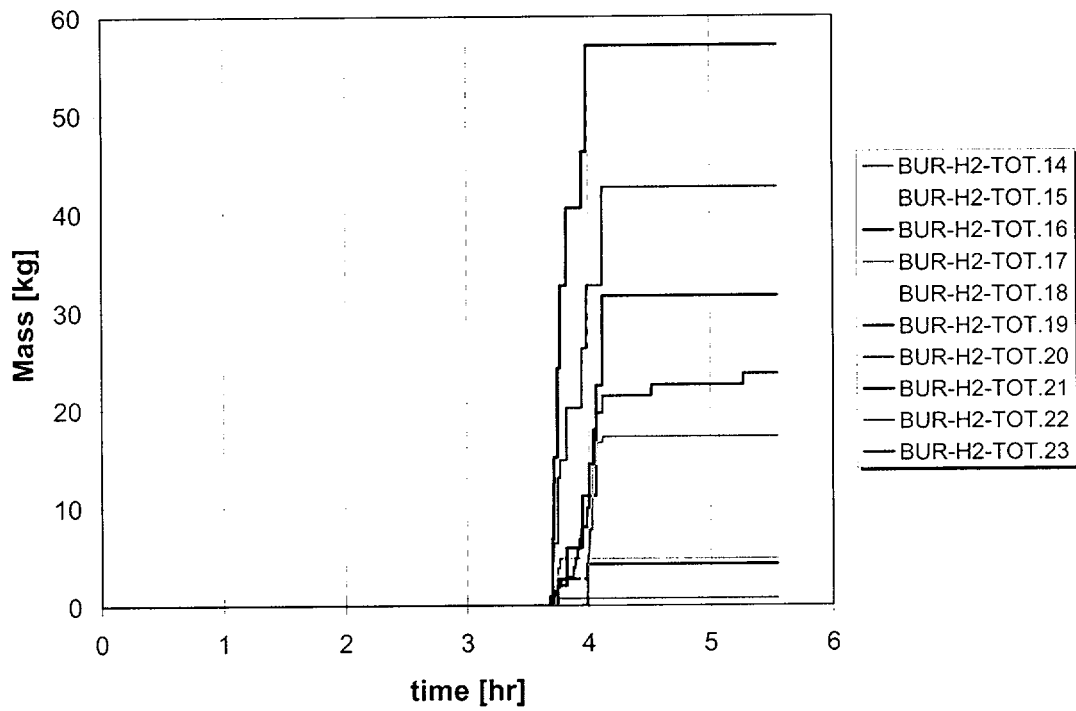


Figure 35 Ice condenser hydrogen burned, power to igniters only (26-cell model).

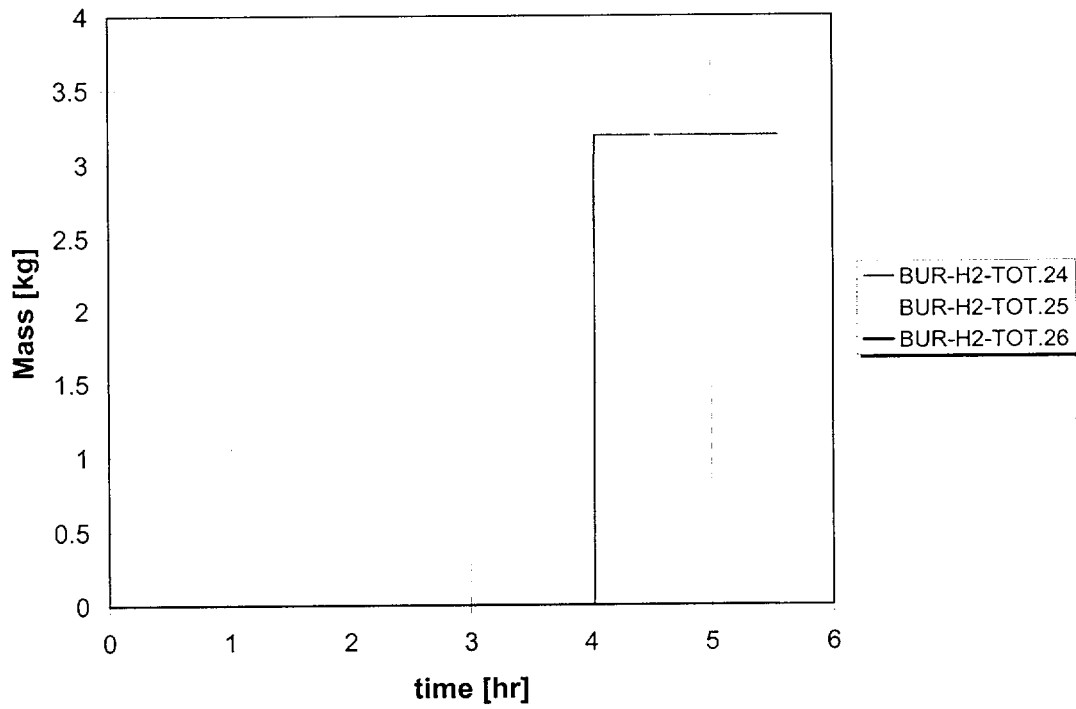


Figure 36 Upper containment hydrogen burned, power to igniters only (26-cell model).

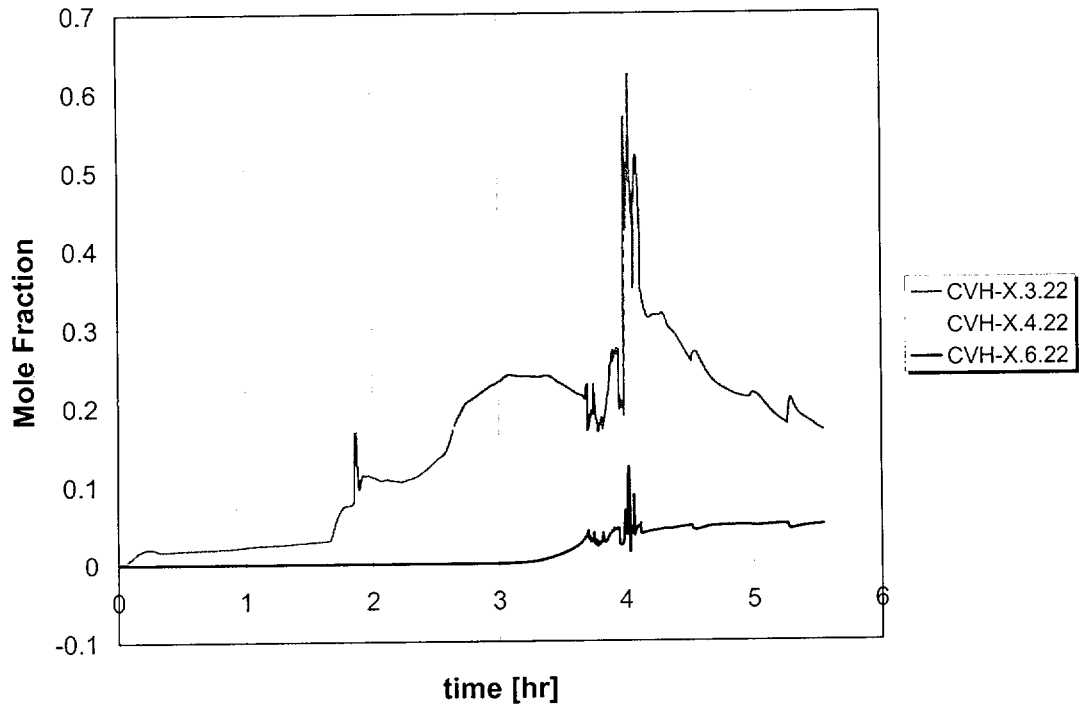


Figure 37 Upper plenum gas/steam concentration, power to igniters only (26-cell model).

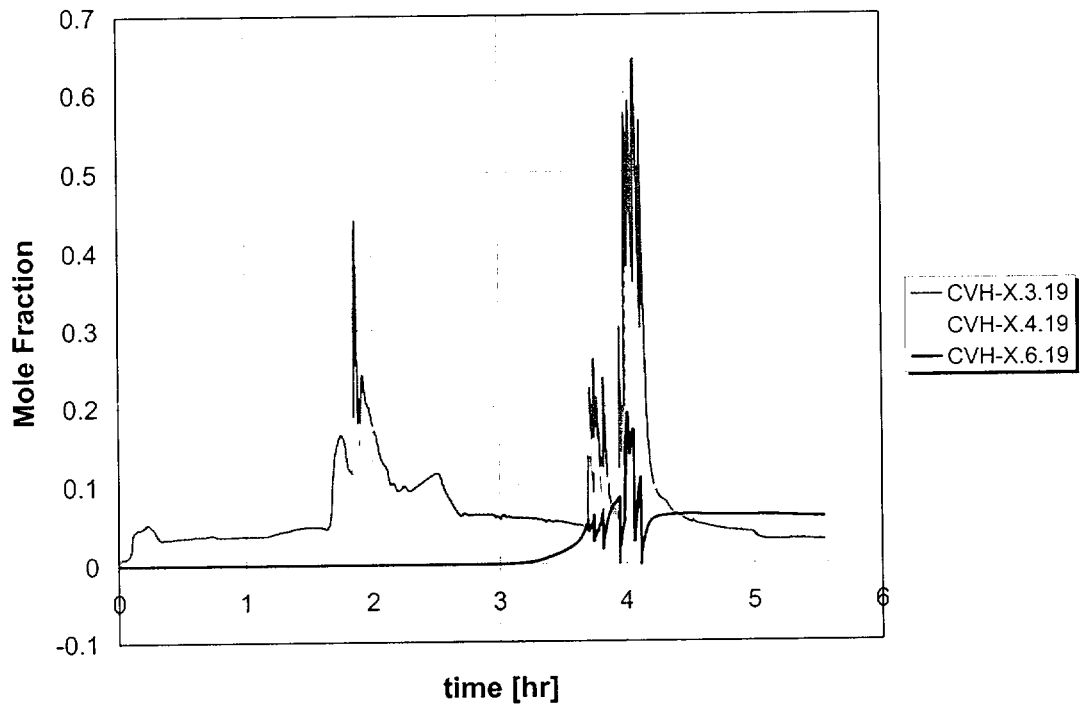


Figure 38 Ice bed gas/steam concentration, power to igniters only (26-cell model).

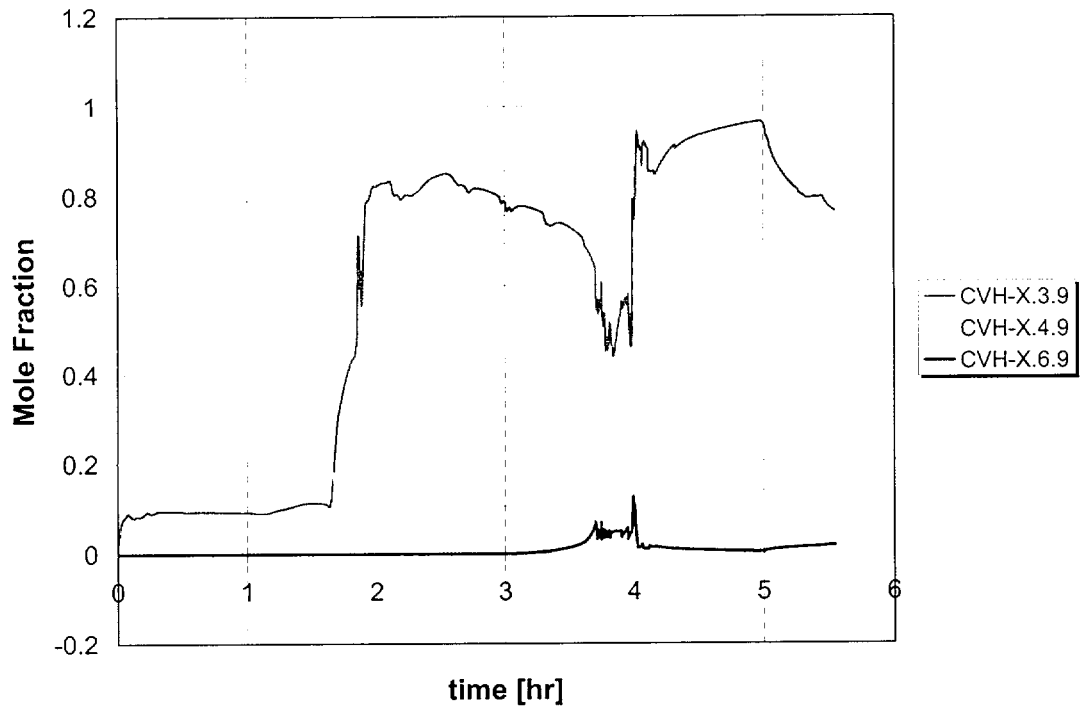


Figure 39 Lower containment gas/steam concentration, power to igniters only (26-cell model).

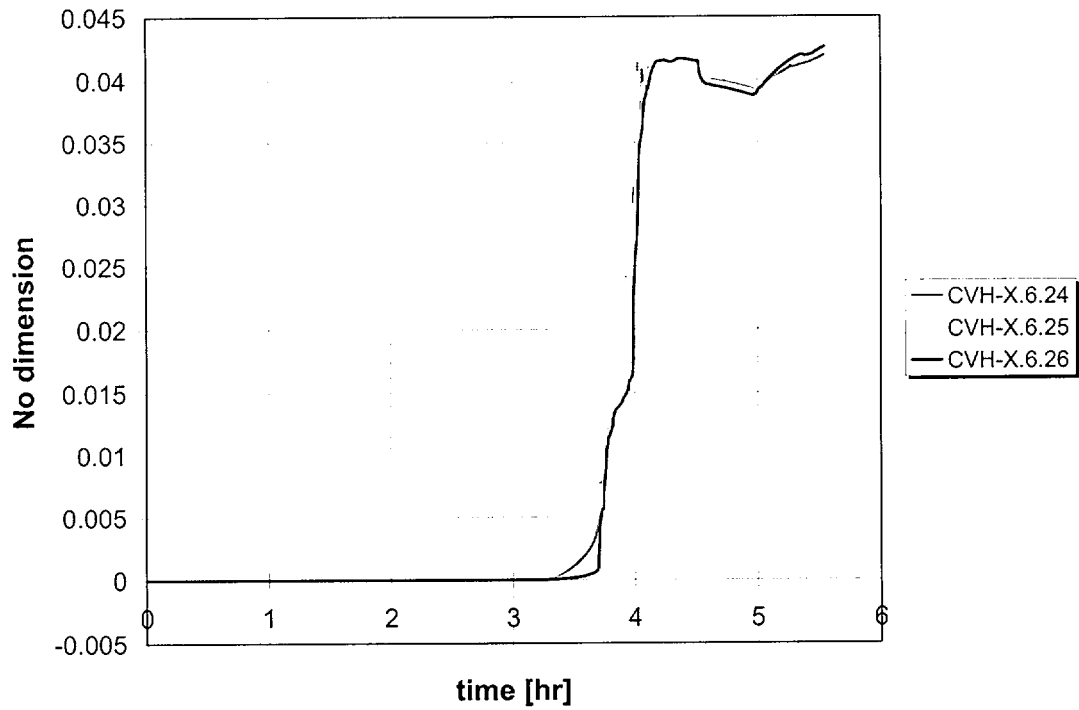


Figure 40 Upper containment hydrogen concentration , power to igniters only (26-cell model).

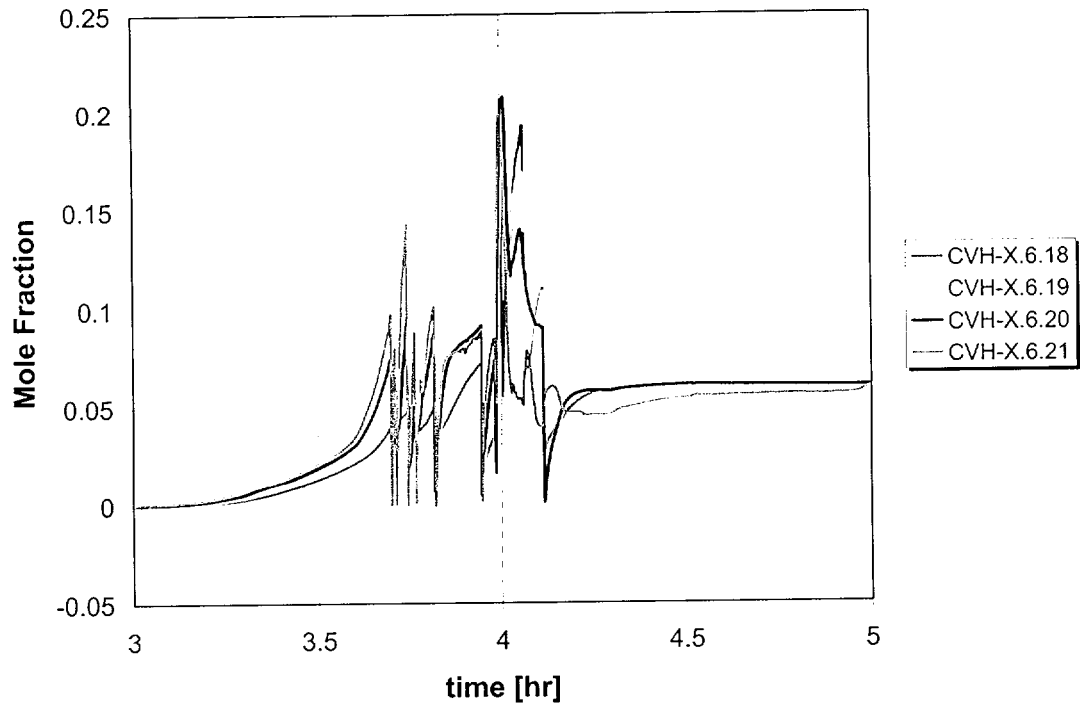


Figure 41 Ice bed hydrogen concentrations, power to igniters only (26-cell model).

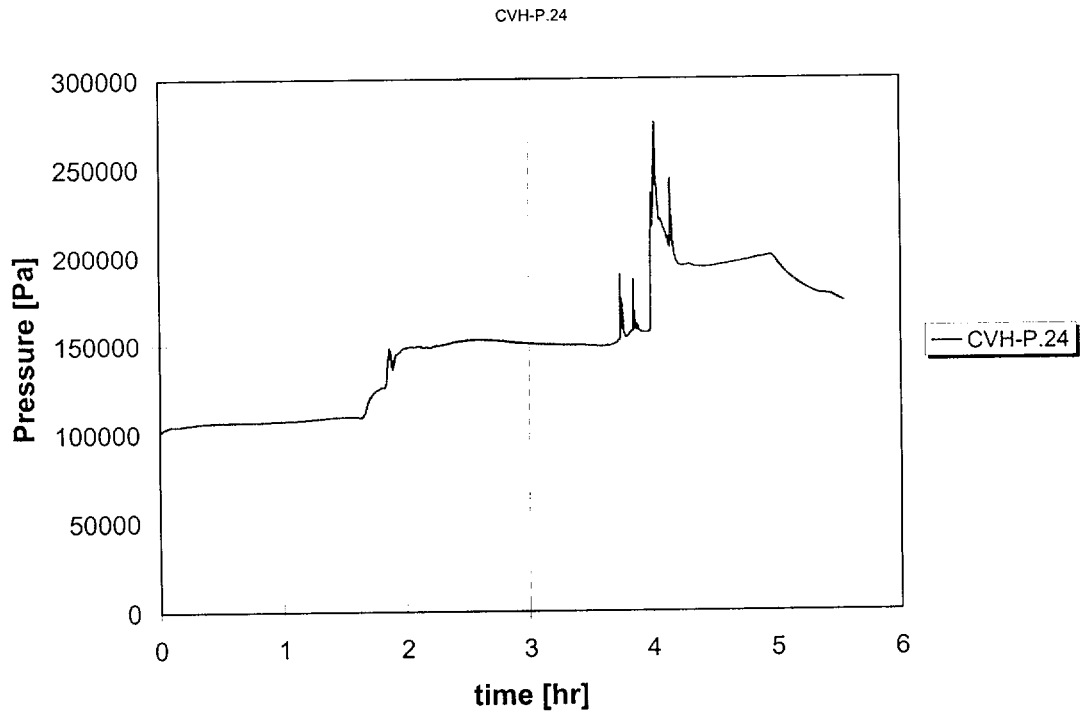


Figure 42 Upper containment pressure, power to igniters only (38-cell model).

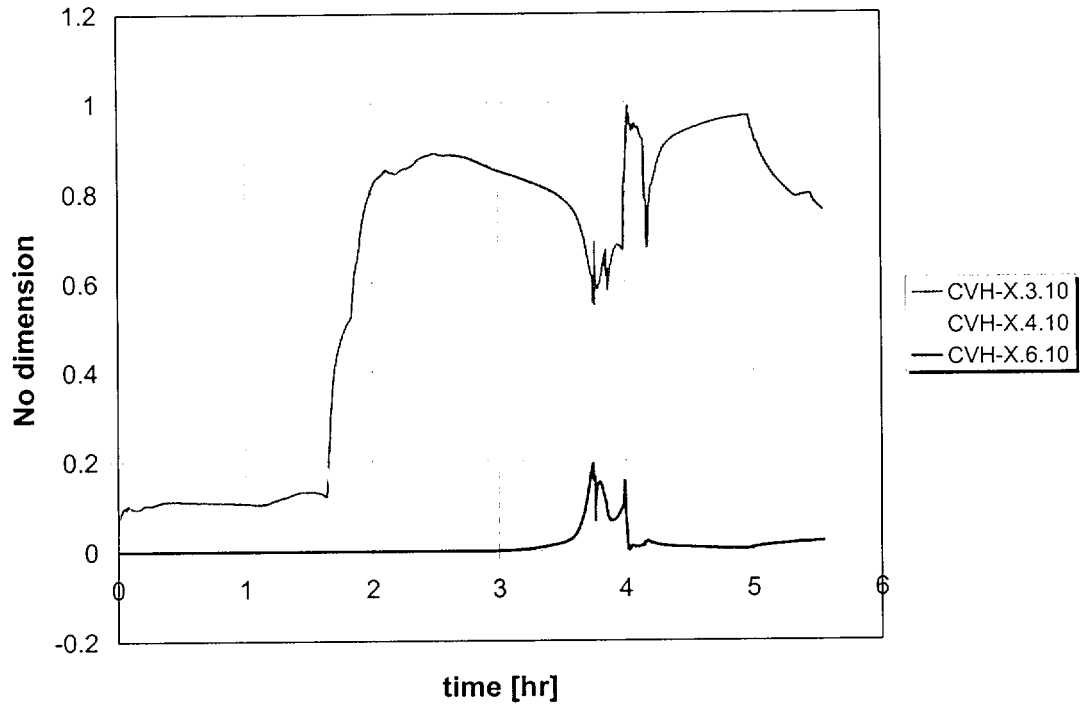


Figure 43 Lower containment gas/steam concentrations, power to igniters only (38-cell model).

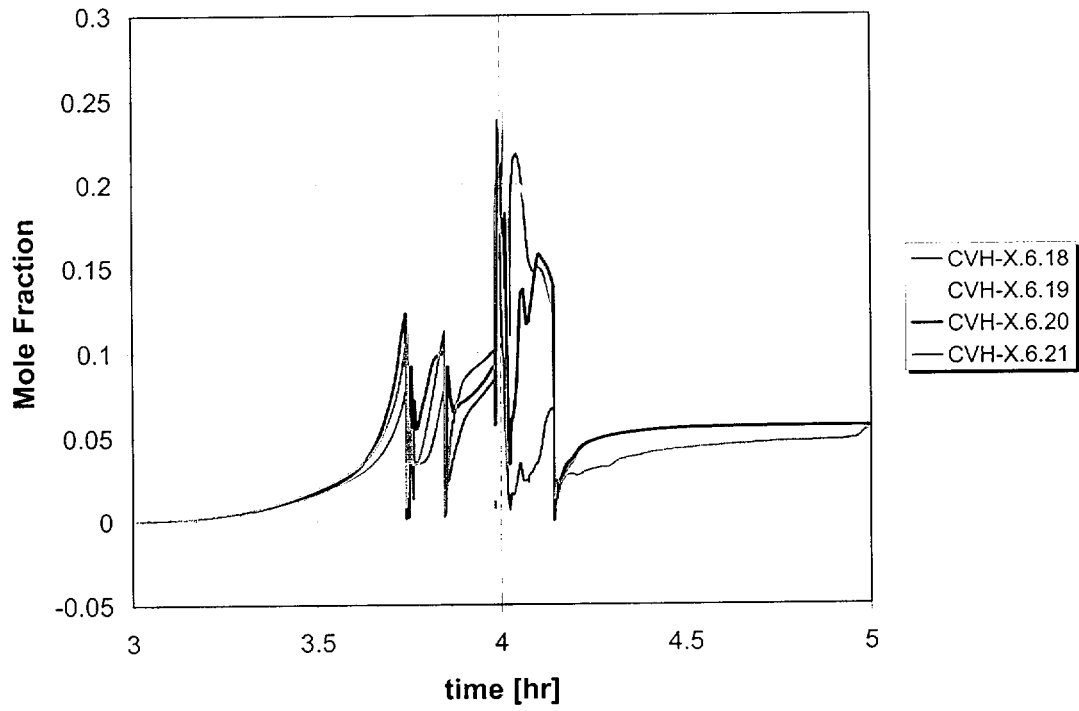


Figure 44 Hydrogen concentration in lower ice bed, power to igniters only (38-cell model).

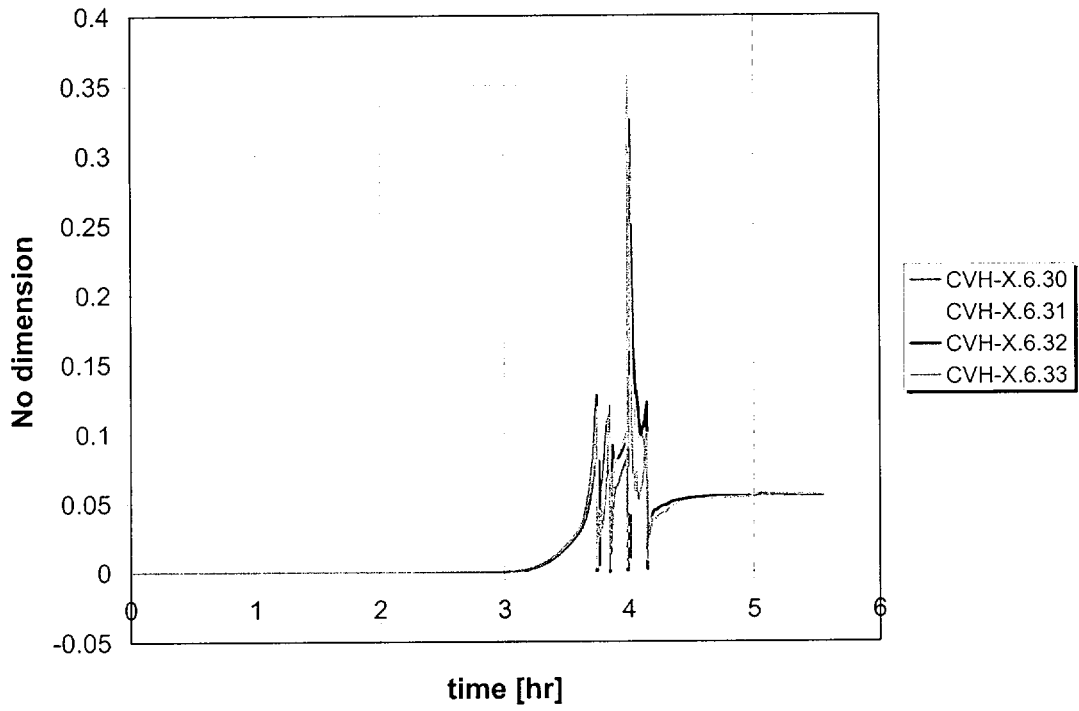


Figure 45 Hydrogen concentration in the upper ice bed, power to igniters only (38-cell model).

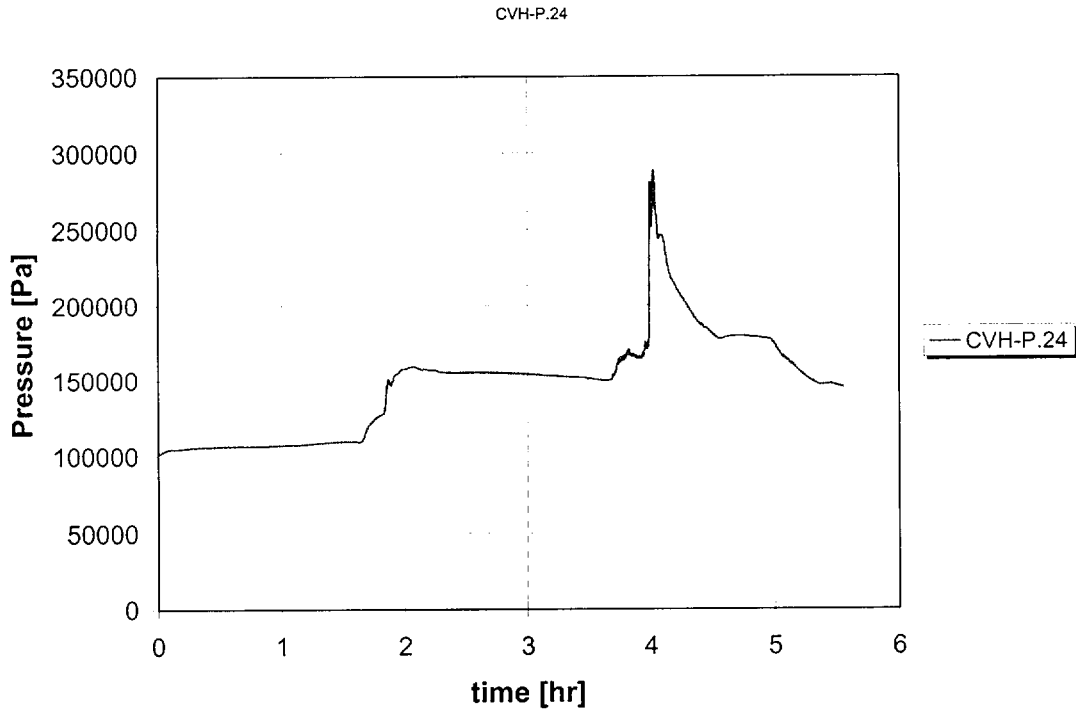


Figure 46 Upper containment pressure, power to igniters and fans (26-cell model).

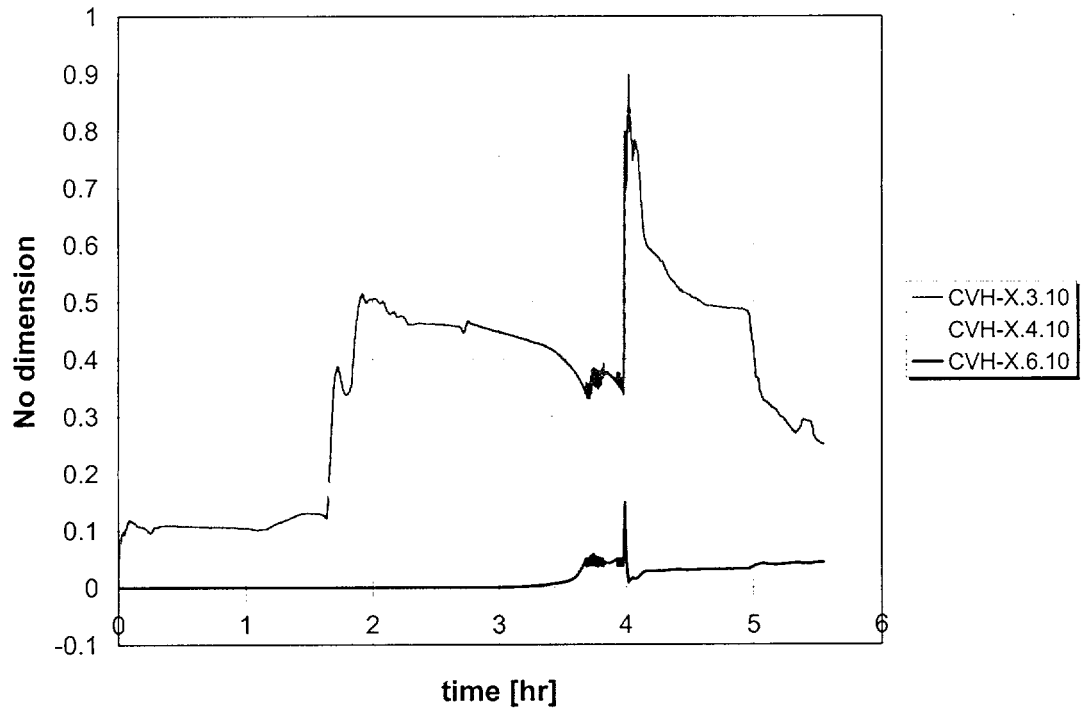


Figure 47 Compartment #10 gas/steam concentration, power to igniters and fans (26-cell model).

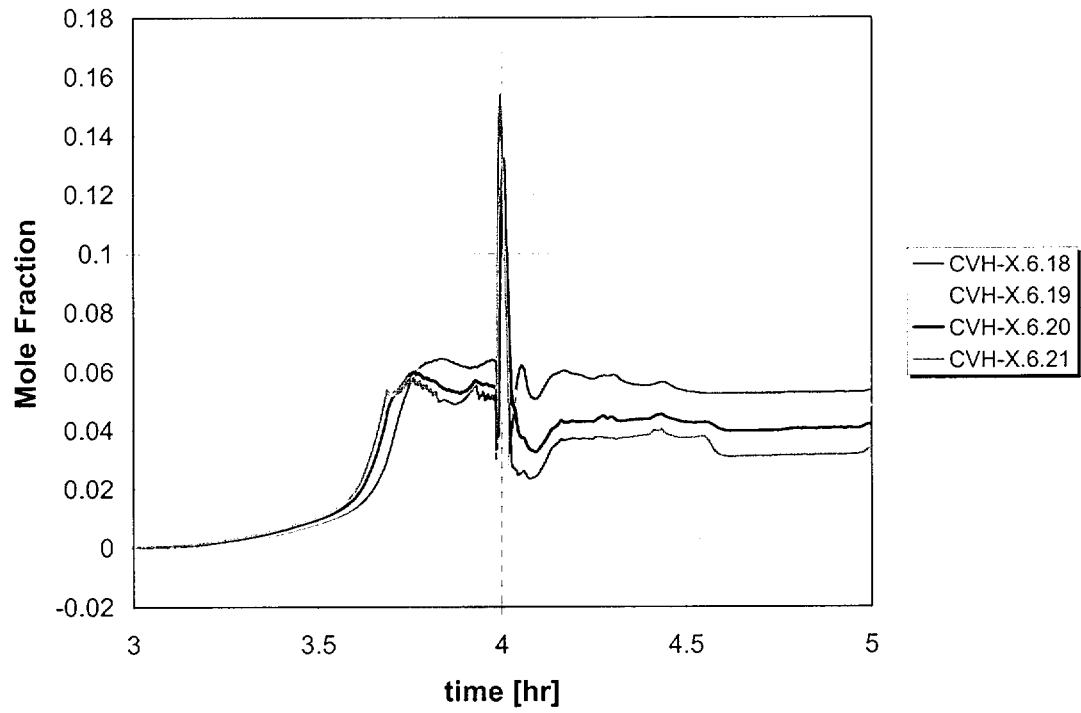


Figure 48 Hydrogen concentrations in the ice bed, power to igniters and fans (26-cell model)